CHAPTER 4

Interplay of Structural and Electronic Properties

S. Kagoshima, R. Kato, H. Fukuyama, H. Seo and H. Kino

University of Tokyo, Tokyo, Japan

This chapter provides the overview of the structure-electronic-property relationship of synthetic metals. It is organized in three parts. The first part (by R. Kato) is mainly devoted to the influence of the molecular arrangement on the electronic structure. Two main topics are discussed: the role of dimensionality and the "single-band"-versus-"multi-band" systems. The second part (by S. Kagoshima) deals with the structural changes predominantly caused by the low-dimensionality of electron system. It is a "re-visitation" of the Peierls and Spin-Peierls transition, and anion ordering. TCNQ- and TMTSF-based systems are used as "textbook" examples because they are the most studied systems. The sub-section 2.5 offers a more current discussion on the interplay of various instabilities in DCNQI–Cu compounds. The third part (by H. Fukuyama, H. Seo and H. Kino) gives a proposition for unifying classification on various ground states observed in organic metals.

1. Molecule, Molecular Arrangement, and Electronic Structure

Molecular conductors exhibit a variety of physical properties that can be systematically understood on the basis of simple and clear electronic structures. Recent advances in angle-dependent magnetoresistance studies on molecular conductors have revealed that the simple tight-binding band calculation is very useful (but not almighty) to describe the Fermi surface topology [1, 2]. The variety observed in electronic structures heavily depends on the packing

Donor

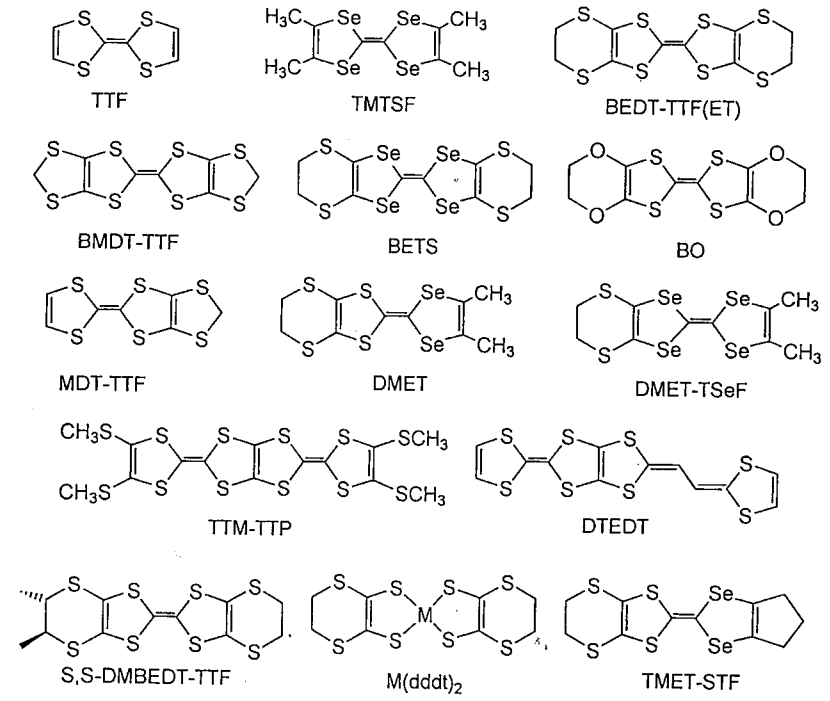

Acceptor

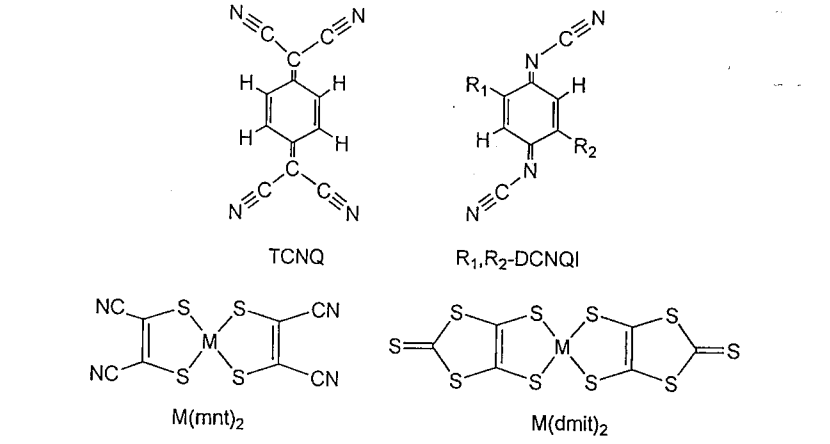

Figure 1 Examples of component molecules for molecular conductors.

arrangement of the molecule. Several molecules that construct molecular conductors are shown in Fig. 1. The molecular conductor is composed of cation radicals from donor molecules and/or anion radicals from acceptor molecules accompanied by counter ions. Conduction electrons are carried through the radical part. Plenty of synthetic works have revealed that small change in chemistry can provide drastic differences in physical properties. Increasing attention is directed to the fine control of solid state properties with chemical or structural modifications performed at radical parts and at counter ions. From the viewpoint of the electronic structure, there have been two major trends in the development of the molecular conductors, according to which we briefly overview the chemical or structural aspects of the molecular conductors in this section.

1.1. From "one-dimensional" *to* "higher-dimensional"

At birth, the molecular metal was the one-dimensional metal. KCP and TTF–TCNQ are typical examples. The one-dimensional metal, however, is not a "metal" in the low temperature region due to the instability of the planar Fermi surface. Of course, this instability has provided rich physics [3], but is not favorable to the superconductivity. Therefore, chemists made efforts to increase the dimensionality of the electronic structure by the chemical modification with great success. The first organic superconducting system, the Bechgaard salt, is a quasi-one-dimensional system [4]. BEDT–TTF salts, the second-generation organic superconductors, have typical two-dimensional Fermi surfaces [5]. Three-dimensional Fermi surface has been found in the DCNQI–Cu salt [6].

It was thought to be difficult to obtain higher-dimensional molecular conductors, because component molecules are (almost) planar and the $p\pi$ (or dz^2 in KCP) orbital shows strong anisotropy. The face-to-face stacking (column) is a favorable architecture and tends to provide the one-dimensional conduction path. If we start from the column structure, the easiest way to the higher dimensional system is enhancement of intercolumn interactions. Replacement of S atoms in the TTF skeleton with larger Se atoms is an effective method. In $(TMTSF)_2X$, short Se···Se contacts enhance the intercolumn interaction up to about 1/10 of the intracolumn interaction (Fig. 2). The Fermi surface of this system is a pair of distorted planes, which has been analyzed quantitatively through the angle dependent magnetoresistance oscillation [2].

The first two-dimensional metal derived from the π-acceptor molecule, α-Et_2Me_2N $[Ni(dmit)_2]_2$, has shown another way to the higher dimensional system based on the face-to-face stacking architecture [7]. Figure 3 shows the crystal structure. The repeating unit along the *c* axis consists of four $Ni(dmit)_2$ molecules. There are two types of overlapping modes, I (A···B) and II (A···C). The mode I, where *one* molecule overlaps with *two* molecules, is of special interest. The transverse intermolecular interaction for the $Ni(dmit)_2$ molecule is

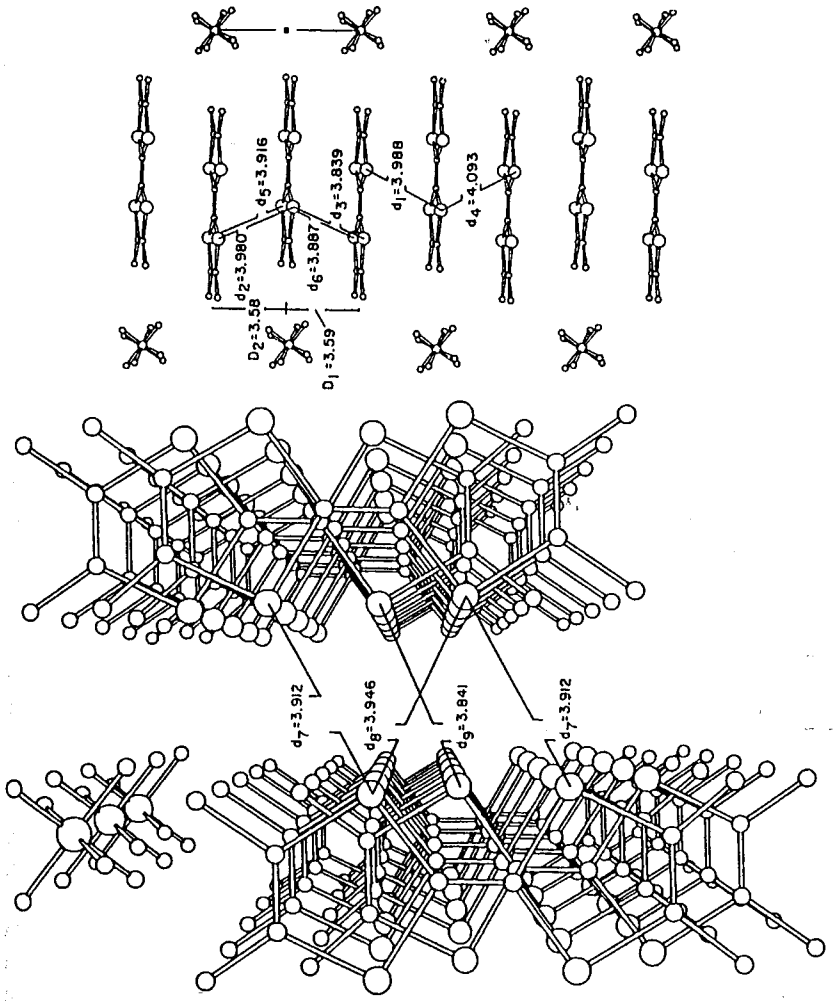

Figure 2 Crystal structure of $(TMTSF)_2PF_6$. (Reproduced from Fig. 1 in *Accounts Chem. Res.* 18 (1985) 261.)

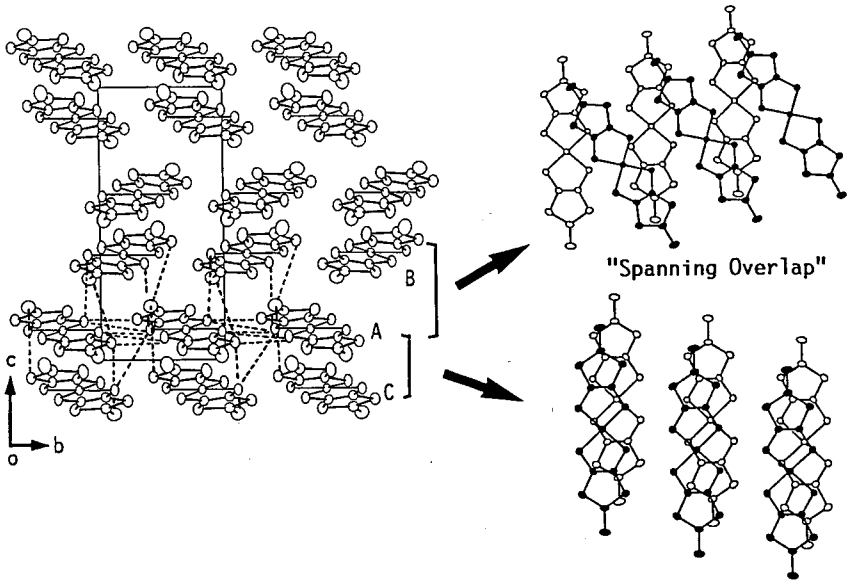

Figure 3 Crystal structure of α-$Et_2Me_2N[Ni(dmit)_2]_2$.

rather poor due to the b_{2g} symmetry of the LUMO, which is unfavorable for the enhancement of the interstack interaction. The mode I overlap ("spanning overlap"), however, provides a two-dimensional conduction path parallel to the *bc* plane. Indeed, the Fermi surface of this compound was found to be two-dimensional [8]. Molecular design toward such a type of molecular arrangement has been proposed for axially substituted phthalocyanine neutral radicals [9].

The organic donor molecule BEDT–TTF (ET) removed an impression that the π molecule prefers the face-to-face stacking structure, which was "one giant leap" for the molecular conductor. Typical two-dimensional molecular arrangements (designated β, θ, and κ) derived from the ET molecule are shown in Fig. 4 with calculated Fermi surfaces. The β-type arrangement is composed of loosely stacked ET dimers [10]. The short S···S contacts are observed between stacks, while there is no short S···S contact within the stacks. Such a structural feature, which was not observed in the regular column structures, provides two-dimensional interdimer interactions. There are many variations of the β-type arrangement (β′, β″, ··· etc.), each of which shows different dimensionality in its electronic structure. This means that the two-dimensional electronic structure derived from the β-type arrangement is not so stable against the packing modification. The intermolecular overlap integral between HOMOs was calculated for a pair of ET molecules where two molecules take various arrangements with keeping their long axes and their molecular planes parallel to each other (as is the case of the β-series arrangements) [11]. This map of the overlap integral as a function of cylindrical coordinates indicates that the

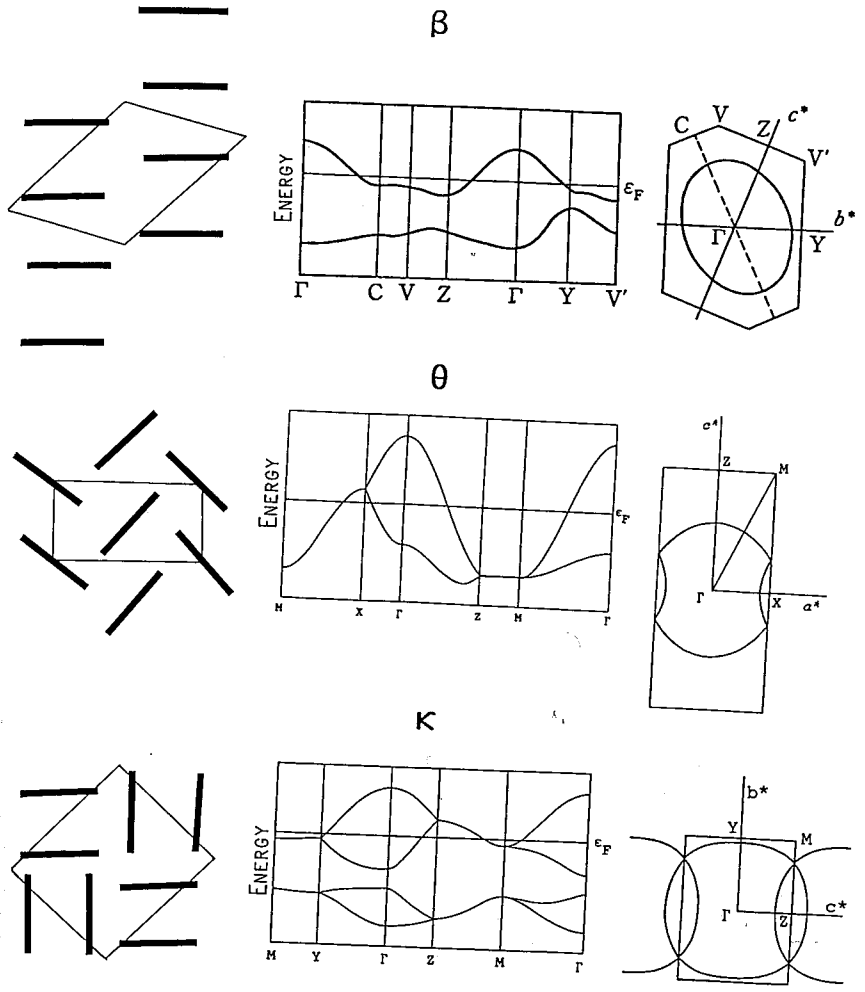

Figure 4 Schematic molecular arrangements of ET molecules (end-on projection) in β-$(ET)_2I_3$, θ-$(ET)_2I_3$ (averaged structure), and κ-$(ET)_2I_3$ with calculated Fermi surfaces.

intermolecular overlap integral changes sensitively to the relative arrangement of two ET molecules.

In the θ-type arrangement, each ET molecule is surrounded by six ET molecules almost isotropically [12]. There is not any face-to-face overlap of ET molecules, which indicates that the θ-type arrangement largely deviates from the face-to-face column. The dihedral angle (θ) between donor molecules can be tuned by the choice of the counter anion. Simple calculations indicate that an increase of the dihedral angle θ leads to a significant decrease of the transfer integral in the transverse direction. In the general phase diagram for the θ-ET

salts, the low-temperature ground state varies from insulating, to superconducting, to metallic with decreasing the electronic correlation parameter U/W, where U is the effective on-site Coulomb energy and W is the band width [13]. In contrast to the β-type arrangement, the shape of the Fermi surface derived from the θ-type arrangement is not so sensitive to the dihedral angle θ. The θ-type is often compared with the donor arrangements observed in α-$(ET)_2I_3$ [14] and α-$(ET)_2MHg(SCN)_4$ (M = K, NH_4, Rb, Tl) [15]. All of them are based on the "herring bone" arrangement and short S···S contacts in the transverse direction. The periodic patterns of the ET arrangement along the molecular longitudinal axis in α-$(ET)_2MHg(SCN)_4$ and in α-$(ET)_2I_3$ are different from that in the θ-salts. In each case of α-$(ET)_2I_3$ and α-$(ET)_2MHg(SCN)_4$, the crystal contains three crystallographically independent ET molecules, two of which are located on non-equivalent inversion centers. X-ray crystal structure analysis suggests that the formal charges on these ET molecules are different to each other in α-$(ET)_2I_3$, while there is no meaningful difference of the formal charge in α-$(ET)_2MHg(SCN)_4$. The essential feature of the Fermi surface for α-$(ET)_2MHg(SCN)_4$ is similar to that for the θ-type. A removal of the degeneracy due to the subtle structural distortion, however, resolves a cylindrical Fermi surface into the open and closed pieces. α-$(ET)_2I_3$ shows a semi-metallic band structure with slight band overlap. The interrelation between the electronic structure of α-$(ET)_2MHg(SCN)_4$ and that of α-$(ET)_2I_3$ can be explained in terms of the change of the characteristic intermolecular interaction [16].

The κ-type arrangement contains no distinguishable stack [17]. The crystal contains conducting layers, each of which is composed of orthogonally arranged ET dimers. Interdimer interactions are two-dimensional and provide a cylindrical Fermi surface. Many ET-based organic superconductors with rather high transition temperatures are known to possess the κ-type arrangement. The κ-ET salts can be mapped in the general phase diagram that is composed of four phases; paramagnetic metal, paramagnetic insulator, superconductor, and antiferromagnetic insulator [18]. This phase diagram is also understood in terms of the electronic correlation parameter which is tuned by the degree of the dimerization. It should be noted that other donor molecules (for example, BETS, MDT–TTF, BMDT–TTF, TTP's, *S,S*-DMBEDT–TTF, DMET, and so on) also exhibit the κ-like arrangements [19].

An important feature of the ET molecule is the outer six-membered heterorings that expand the π-conjugating system of the TTF skeleton and enhance intermolecular S···S contacts in the transverse direction. This understanding led to an idea that adjustments of periphery of the molecule considering sizes of the heterorings and the chalcogen atoms are effective in the control of the dimensionality [20]. Two typical examples are BETS and TTPs. In the BETS molecule, the fulvene S atoms in the BEDT–TTF molecule are replaced by larger Se atoms [21]. In the transverse direction, the expanse of Se orbitals in the five-membered ring is almost the same with that of S orbitals in the six-membered ring, that is, the peripheral "surface" of this molecule is almost flat (Fig. 5). This

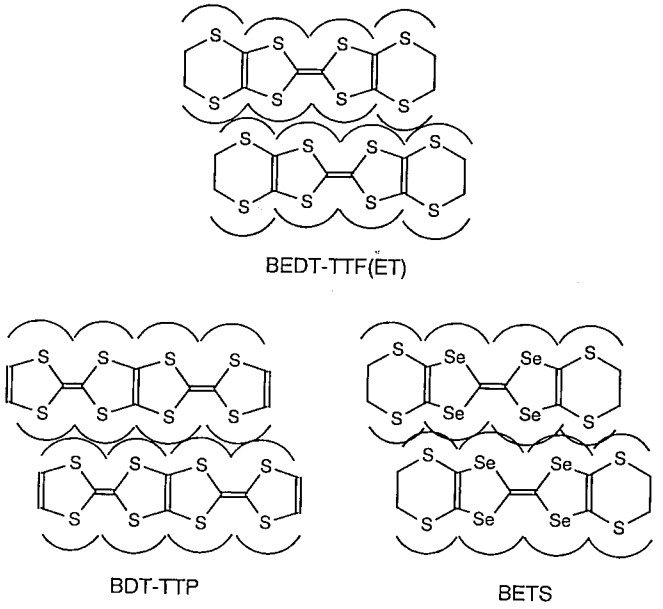

Figure 5 Side-by-side intermolecular interactions in ET, BETS, and TTP.

feature is quite suitable for the enhancement of the transverse overlap. A number of BETS salts with two-dimensional electronic structures were prepared and found to exhibit metallic or superconducting behaviors. The λ-type arrangement was first observed in the BETS salts with tetrahedral anions [22]. This type of arrangement is a four-fold quasi-stacking (Fig. 6). The short chalcogen···chalcogen contacts are found between stacks, rather than within the stacks. The Fermi surface derived from this type of molecular arrangement is also two-dimensional. In general, the electrical properties of molecular conductors are strongly influenced by the disorder in the crystal. In the alloy system λ-$(BETS)_2GaX_zY_{4-z}$, however, the disorder effect on the resistivity behavior is not serious, which suggests strong tendency of BETS to retain the metallic state [23].

The fundamental framework of the TTP-type donors is a bis-fused TTF unit where the size of all the heterorings is unified [24]. This also provides flat peripheral "surface" (Fig. 5). The TTP-type donors gave a large number of cation radical salts that retain metallic conductivity down to low temperatures. They exhibit various types of two-dimensional molecular arrangements including β-, θ-, and κ-types [25]. Although any superconductors have not been derived from the usual TTP-type donors, the vinylogous analog DTEDT was found to form a superconducting salt $(DTEDT)_3Au(CN)_2$ [26]. This salt contains uniform stacks of donors that lead to a "uniform β-type" arrangement. Owing to the uniform stacking and the low degree of oxidation, the calculated Fermi surface is two-dimensional.

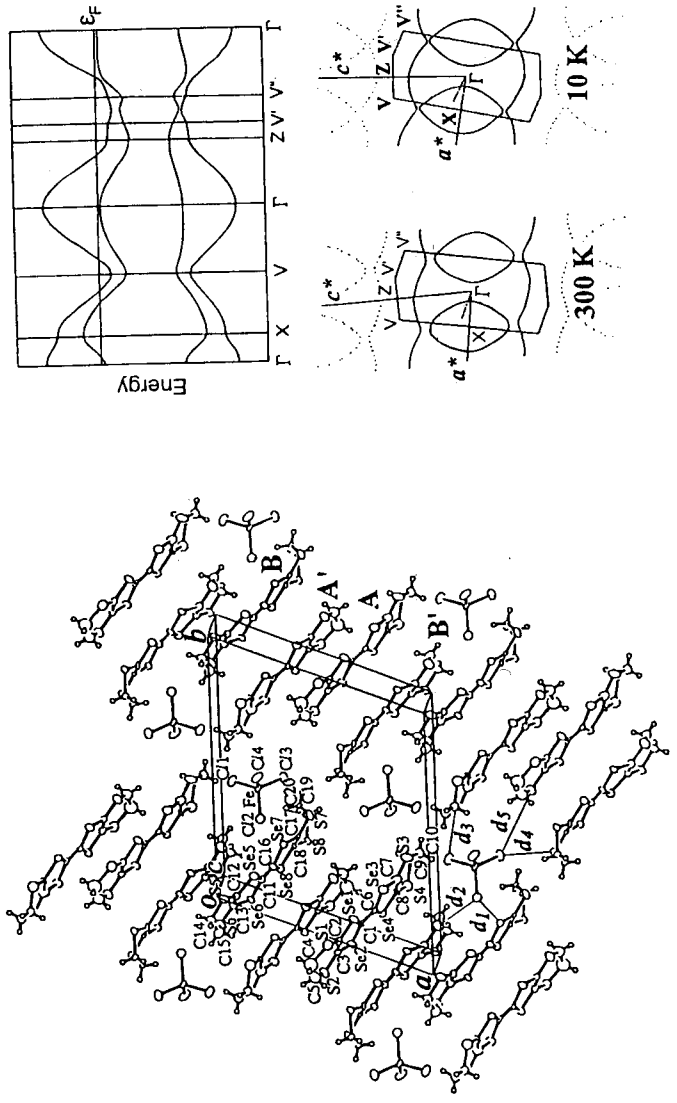

Figure 6 Crystal structure, calculated band structure and Fermi surface for λ-$(BETS)_2GaCl_4$. (Reproduced from Figs. 10, 14 in *J. Am. Chem.Soc.*, 118 (1996) 368)

It should be added that the expansion of the π-conjugating system and/or the introduction of Se atoms with greater polarizability (as shown in BETS or TTPs) reduce the effective on-site Coulomb energy *U*. For example, the *U* values for the TTP-type donors estimated from electrochemical and optical measurements are considerably small. $(TTM–TTP)I_3$ is a 1:1 salt with a highly one-dimensional half-filled band. Although 1:1 salts were believed to be non-metal due to the Coulomb interaction (Mott-insulator), this salt shows metallic behavior down to about 160 K. This system is regarded as a small-*U* case of a one-dimensional conductor with an inherently half-filled band [27].

Another very interesting two-dimensional molecular arrangement is the τ-type arrangement derived from some unsymmetrical donor molecules [19, 28]. Figure 7 shows the crystal structure of τ-(P-(S,S)-DMEDT–TTF)$_2$(AuBr$_2$)$_1$(AuBr$_2$)$_{\sim 0.75}$. In the crystal, the linear anions penetrate into the donor layer. Each anion is surrounded by four donor molecules that are arranged orthogonally and connected by short S···S and S···N contacts. The intermolecular interactions are isotropic in the donor layer. The interactions between parallel donors are weaker

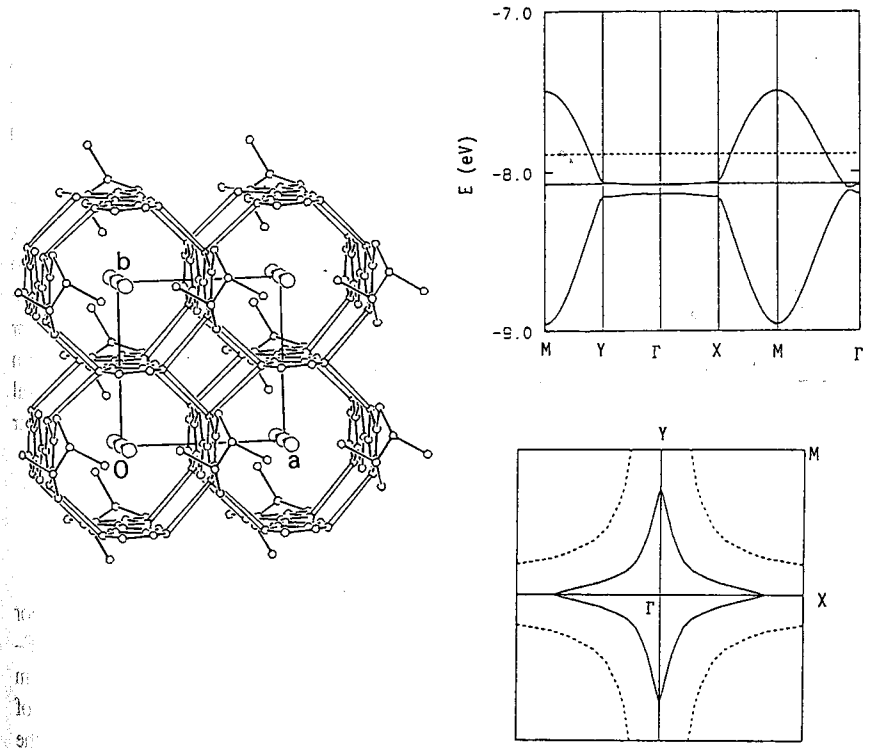

Figure 7 Crystal structure, band structure and calculated Fermi surface for τ-(P-(S,S)-DMEDT–TTF)$_2$(AuBr$_2$)$_1$(AuBr$_2$)$_{\sim 0.75}$. (Reproduced from Figs. 1, 2 in *Solid State Commun.*, 95 (1995) 211)

than those between perpendicular ones. Therefore, the tight-binding band calculation gives almost zero (Y-Γ-X) and large (X(Y)-M-Γ) dispersions along the different directions in the reciprocal space. This characteristic dispersion provides a star-like shaped Fermi surface (Fig. 7).

The expansion of the π-conjugating system with outer heterorings, the idea presented by the ET molecule, can be applied to 1,2-dithiolene metal complexes with the donor character. For example, the $M(dddt)_2$ (dddt = 5,6-dihydro-1,4-dithiin-2,3-dithiol; M = Ni, Pd, Pt, Au) molecule, where the central C=C double bond in ET is replaced by the transition metal, exhibits various molecular arrangements, some of which are similar to those found in the ET salts [29]. In the frontier molecular orbital of the 1,2-dithiolene complexes, the 3p orbitals of S atoms in the ligand show a significant contribution. In this sense, the molecular design for the 1,2-dithiolene complexes can be discussed in common with that for the organic π molecules.

The DCNQI–Cu salt indicates another way to the higher dimensional system with the use of the coordination bond [30]. The crystal structure of the anion radical salt $(DCNQI)_2Cu$ is shown in Fig. 8. Planar DCNQI molecules stack to form one-dimensional columns. These DCNQI columns are interconnected to each other through tetrahedrally coordinated Cu ions to form the three-dimensional DCNQI–Cu network. If there is no interaction between Cu and DCNQI, this structure gives only one-dimensional π (LUMO) band, as is the case of ordinary molecular conductors. But, in this case, the Cu is in the mixed valence state [31] and provides three-dimensional band structure.

Figure 9 shows Fermi surface of $(DMe–DCNQI)_2Cu$ calculated with the tight-binding approximation. This Fermi surface has been confirmed by the dHvA measurement [5]. The first principles band calculation for this system was also performed and gave a sufficient result [32]. In this system, there is a coexistence of the purely one-dimensional Fermi surface, FS1, which comes from organic π bands, and three-dimensional Fermi surface, FS3 which originates mainly from the 3d band. This unique electronic structure originates from the tetrahedral coordination geometry of the copper and the interplay between d orbitals and pπ orbitals.

1.2. From "single component" *to* "multi component"

Molecular conductors at the first stage were single component systems. For example, the conduction band in KCP is a one-dimensional dz^2 band. TTF–TCNQ has a HOMO band of TTF and a LUMO band of TCNQ, but both of them are one-dimensional pure π bands. Recently, however, increasing number of interesting systems which have "two" bands with different characters near the Fermi level have been reported: for example, the DCNQI–Cu salt with π and (itinerant) d bands, $Pd(dmit)_2$ salts with a two-dimensional HOMO band and a one-dimensional LUMO band, the organic superconductor $(TMET–STF)_2BF_4$

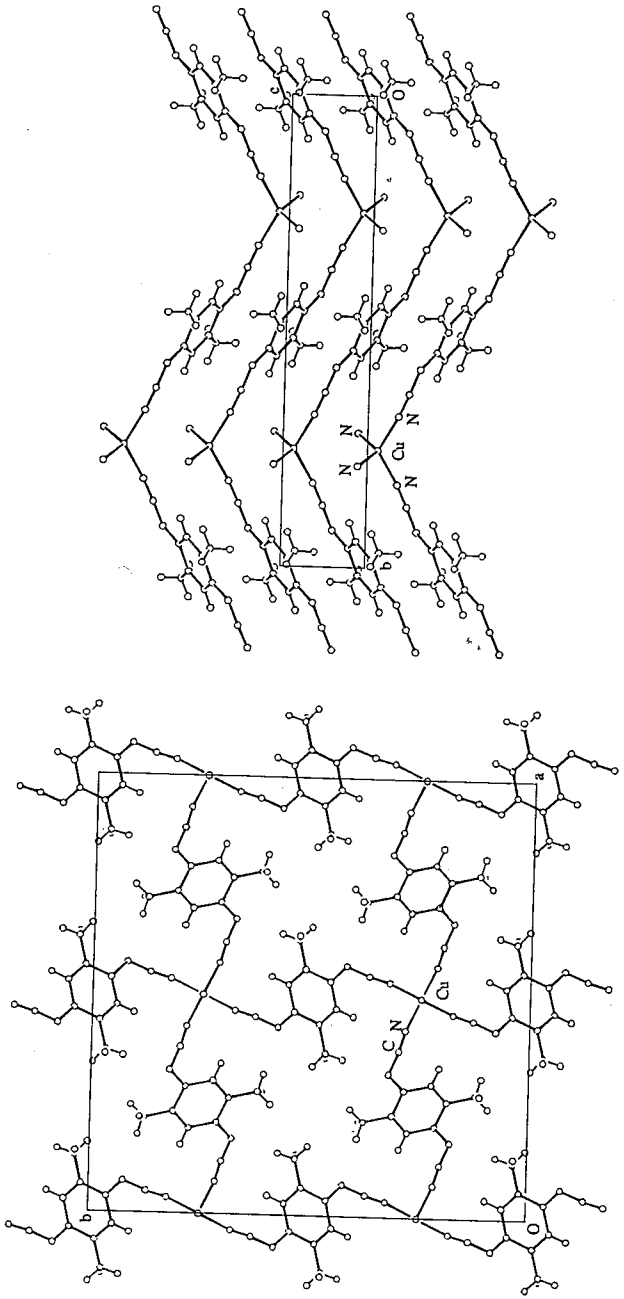

Figure 8 Crystal structure of (DMe-DCNQI)2Cu.

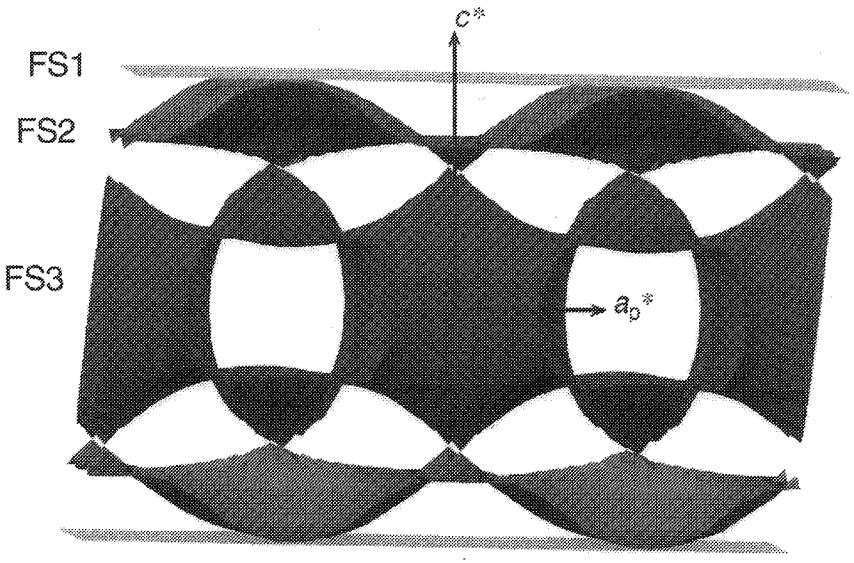

Figure 9 Calculated Fermi surface of (DMe–DCNQI)$_2$Cu. (Reproduced from Fig. 2 in *Mol. Cryst. Liq. Cryst.*, 284 (1996) 183.)

with a two-dimensional HOMO band and a one-dimensional HOMO band [33]. On the other hand, in the BETS salt with $FeCl_4$, localized d spins on the Fe^{3+} ions interact with itinerant π electrons.

We have mentioned that molecular conductors exhibit simple and clear electronic structures where the simple tight-binding method is a good approximation. In most molecular metals, the conduction band originates from only one frontier molecular orbital (HOMO for donor, LUMO for acceptor). This is because the inter-molecular transfer energy is smaller than energy differences among molecular orbitals. However, it is possible to locate two bands with different characters near the Fermi level. In some cases, interplay of these two bands provides unique physical properties. The typical example is the (R_1, R_2–DCNQI)$_2$Cu system.

As mentioned in 1.1, the conduction band of the DCNQI–Cu system is composed of the d (d_{xy}) orbital of Cu and the LUMO of DCNQI. This system exhibits a variety of physical properties depending on the chemical modification or pressure. Figure 10 is a schematic phase diagram for the DCNQI–Cu system. The electronic states of this system are classified into three types according to transport properties. The type I state is metallic down to the lowest temperature. In the metallic state, the Cu ion is in the mixed-valence state and the valence of Cu is close to 4/3+. Therefore, the one-dimensional organic pπ band interacts with the Cu 3d orbital. An application of pressure transforms the type I state into the type II state. The type II state exhibits a sharp first-order metal-insulator (M-I) transition. The M-I transition of this system is accompanied by a CDW formation

with three-fold lattice distortion [34] and a static charge ordering at the Cu sites (···$Cu^+Cu^+Cu^{2+}$···). Around the critical pressure, the system exhibits a unique metal-insulator-metal, reentrant transition with lowering temperature (type III) [35]. The size of substituents (R_1 and R_2) has the same effect with the pressure

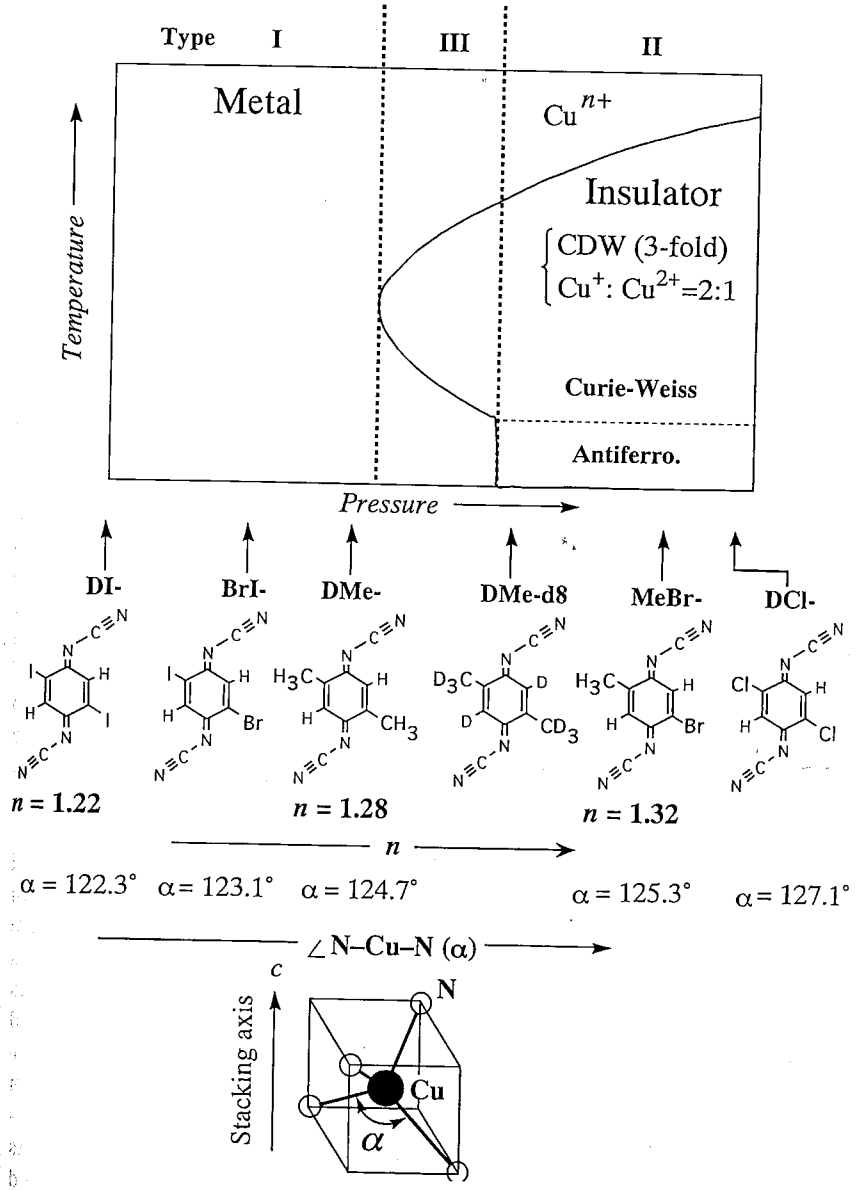

Figure 10 General phase diagram for the DCNQI–Cu salts.

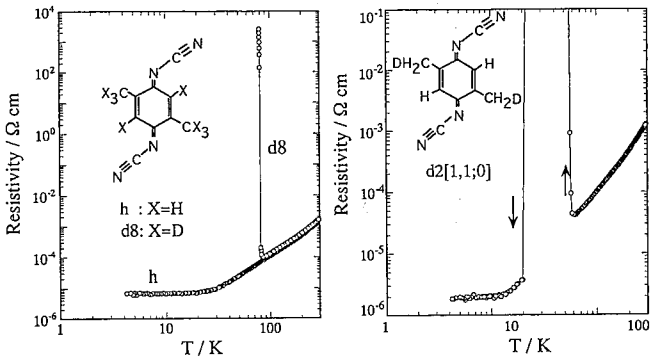

Figure 11 Temperature dependence of the resistivity for pristine (type I), fully deuterated (type II), and selectively deuterated (type III) (DMe–DCNQI)$_2$Cu.

(*chemical pressure* effect). One can notice that the smaller substituents make the metallic state unstable.

Electronic states of (DMe–DCNQI)$_2$Cu ($R_1 = R_2 = CH_3$), which is situated near the boundary, is quite sensitive to the pressure or the chemical modification and fine tuning is possible by a replacement of hydrogen atoms with deuterium atoms [36]. The bond length between carbon and hydrogen is reduced by the deuteration. This gives an effect similar to the application of very low pressure. Figure 11 shows a typical isotope effect. Non-deuterated salt is metallic down to the lowest temperature, while the completely deuterated salt shows very sharp metal-insulator transition. In the metallic phase, temperature-independent Pauli-like behavior is observed. At the metal-insulator transition temperature, there is an abrupt change of the magnetic susceptibility. This indicates an appearance of the local spins at the Cu sites. These local spins obey Currie-Weiss law down to about 30 K. At 8 K, the anti-ferromagnetic transition occurs accompanied by the weak ferromagnetism due to the canting. An introduction of only two deuterium atoms into the methyl groups induces a remarkable reentrant transition (Fig. 11).

Behind such a drastic change of the electronic state by very small modifications, the π-d interaction associated with the ligand field effect plays an important role [37]. The stability of the metallic state is correlated to the valence of Cu in the metallic phase. The valence of Cu estimated by XPS measurements at room temperature is slightly smaller than 4/3+ for each salt and approaches 4/3+ with a decrease in the stability of the metallic state [38]. It should be noted that the averaged valence of Cu in the insulating state is exactly 4/3+ ($Cu^+ : Cu^{2+} = 2:1$) in every case. Theoretical studies have indicated that an interplay of the 3-fold periodic potential associated with the nesting at the one-dimensional LUMO band and the strong correlation at the narrow d band leads to the first-order M-I transition followed by the large hysteresis and the localized spins [39]. In this case, both the CDW on the DCNQI column and the charge

ordering at the Cu sites have the same period and the energy gain is the largest. Therefore, the deviation of the Cu valence from 4/3+ in the metallic state should require the redistribution of the charge for the metal-insulator transition and lower the transition temperature. The valence of Cu can be tuned by the distortion of the coordination tetrahedron represented by the N-Cu-N angle (α). The larger a value makes the valence of Cu larger. This means that the distortion of the coordination tetrahedron induced by the chemical modification or pressure makes the metallic state unstable. A relation between the distortion of the coordination tetrahedron and the valence of Cu is described in the next section. The (DCNQI)$_2$Cu system is an amazing system where very small change in the ligand field can induce a drastic change of the electronic state.

It should be added that some DCNQI–Cu salts, for example (DI–DCNQI)$_2$Cu ($R_1 = R_2 = I$), exhibit a complicated pressure-temperature phase diagram at higher pressure region, which indicates that there should be additional factors that affect the electronic state of the DCNQI–Cu system [40]. In these salts, weak interstack LUMO···LUMO interactions cannot be neglected. The first-principles band calculation for (DI–DCNQI)$_2$Cu suggests that the HOMO bands become strongly dispersive and the LUMO, HOMO and d states are strongly mixed near the Fermi level under much higher pressures [41]. If this is the case, we must consider the HOMO state in addition to the LUMO and d states.

Anion radical salts based on a series of metal dithiolene complexes M(dmit)$_2$ (M = Ni, Pd, Pt) indicate another interesting multi-component system [42, 43]. The M(dmit)$_2$ molecule is a π acceptor which has provided various molecular conductors, including several superconductors [19, 44]. The conduction band in the ordinary molecular conductors based on acceptor molecules is formed by the LUMO. In the M(dmit)$_2$-based conductors, however, the HOMO band also plays an important role and there frequently occurs a "HOMO–LUMO" band inversion [45]. This situation can be tuned by the dimerization of M(dmit)$_2$ molecules.

For an ideal M(dmit)$_2$ molecule with D_{2h} symmetry, the LUMO has b_{2g} symmetry while the HOMO has a_{2u} symmetry. The b_{2g} symmetry of the LUMO is not suitable for the enhancement of the intermolecular interaction along the side-by-side direction. On the other hand, the situation for the HOMO with the a_{2u} symmetry is very similar to that for the HOMO in TTF-type molecules (for example, ET) and leads to the enhanced side-by-side interaction. Therefore, the system contains two bands with different dimensionality; the two-dimensional HOMO band and the one-dimensional LUMO band. Another important factor is that the energy separation ΔE between the HOMO and LUMO levels is small. This is partly because the d metal orbitals cannot mix into the HOMO due to the difference of the symmetry. This small ΔE value becomes important when the M(dmit)$_2$ molecules are strongly dimerized. For each of the HOMO and LUMO states, the dimerization generates the anti-bonding and bonding bands separated by an energy gap. If this dimerization gap is large enough compared with the ΔE value, the anti-bonding HOMO band is located higher than the bonding LUMO band ("HOMO–LUMO" band inversion; Fig. 12). When the formal charge of the

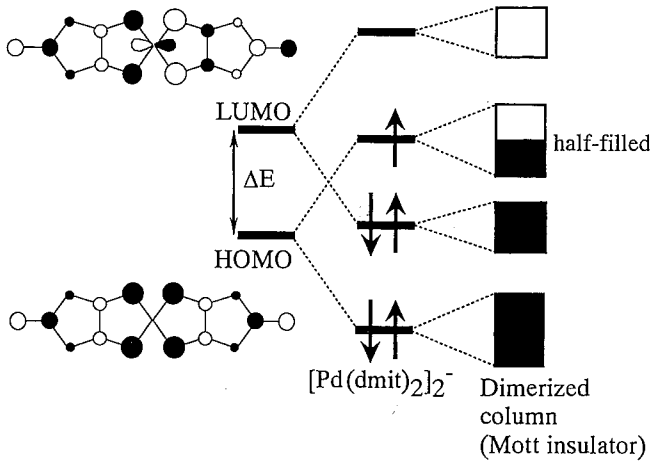

Figure 12 Schematic electronic structure of the dimeric $Pd(dmit)_2$ system with the formal charge of 1/2-.

$M(dmit)_2$ molecule is 1/2-, frequently observed value, the conduction band is the half-filled (anti-bonding) HOMO band. This two-dimensional HOMO band has narrow width as a result of the strong dimerization (the effective band width is correlated to the interdimer transfer integrals). Therefore, the system tends to become a Mott insulator.

In the $Ni(dmit)_2$-based conductors with the stacking arrangement, the dimerization is weak and therefore the conduction band is the (quasi) one-dimensional LUMO band (α-Et_2Me_2N $[Ni(dmit)_2]_2$ is an exceptional case as mentioned in 1.1). On the other hand, most of the $Pd(dmit)_2$-based conductors consist of strongly dimerized $Pd(dmit)_2$ molecules with an eclipsed configuration and very short Pd···Pd distance. The dimerization is a result of the competition between the metal–metal bond and the repulsive chalcogen···chalcogen interactions. These two contributions depend on the spatial extension of the metal and chalcogen orbitals. The strong dimerization leads to the "HOMO–LUMO" band inversion in the $Pd(dmit)_2$-based conductors. For example, reflectance spectra for Me_4As $[Pd(dmit)_2]_2$ and Cs $[Pd(dmit)_2]_2$ revealed that the energy separation ΔE is 0.8–0.9 eV and the anti-bonding HOMO level lies higher than the bonding LUMO level [45]. Estimated band parameters based on the optical data give a picture where strongly dimerized dimers interact to each other with small anisotropy in the conduction layer. In a series of isostructural $\beta'(\beta)$-Me_4Z (Z=N, P, As, Sb) and β'-Et_2Me_2Z (Z=P, As, Sb) salts of $Pd(dmit)_2$ with the formal charge of 1/2-, the conduction band is considered the HOMO band [42]. All these salts show no clear metallic behavior at ambient pressure. Susceptibility, ESR, and NMR measurements indicate that these salts exhibit paramagnetic behavior followed by some anti-ferromagnetic ordering at low temperatures. This suggests that they are Mott-insulators at ambient pressure.

The pressure effect on such a system where the two-dimensional (and half-filled) HOMO band is located immediately above the one-dimensional LUMO band is of special interest. A possible scenario is as follows. The application of the pressure is expected to enhance the inter-dimer transfer integrals. This leads to an increase in band widths for both HOMO and LUMO bands. Therefore, the electronic correlation parameter U/W should be reduced. There should be a pressure above that the HOMO band overlaps with the LUMO band. In this case, the HOMO band is no longer half-filled, which transforms the Mott-insulator to the metal (or the superconductor). But, we must notice that the LUMO character increases at the Fermi level with an increase of pressure. Therefore, at the higher pressures, the one-dimensional nature of the Fermi surface develops and leads to some instability of the metallic state. Indeed, β-Me_4N, β'-Me_4Sb, β'-Et_2Me_2P salts are known to be high-pressure superconductors, and the metallic state that turns unstable under higher pressures is observed in some salts. The pressure effect on the $Pd(dmit)_2$ salts is sensitive to the choice of the cation. Under pressure, this system exhibits a variety of low-temperature ground states (insulating, metallic, and superconducting) according to the cation. This cation dependence suggests that the mechanism of the pressure effect is not so simple [42].

The "HOMO–LUMO" band inversion can also be discussed in the $M(dddt)_2$ system. In contrast to the $M(dmit)_2$ system, however, the "HOMO–LUMO" band inversion in the $M(dddt)_2$ system results in the one-dimensional LUMO band as the conduction band.

Another type of multi component system is the one where itinerant π electrons coexist with localized magnetic moments in counter ions. In such systems, it is possible for π electrons (or holes) to mediate the exchange interaction between the localized magnetic moments. Even if the π electrons are localized, the π electrons can work to couple the magnetic moments through the super-exchange mechanism. There are increasing number of examples; CuPcI [46], $(ET)_3CuBr_4$ [47], $(ET)_4AFe(C_2O_4)_3C_6H_5CN$ (A=H_2O, K, NH_4) [48], λ-$(BETS)_2FeCl_4$ [22] and so on. Among them, λ-$(BETS)_2FeCl_4$ is of special interest. The BETS molecule provides λ-type salts with $GaCl_4^-$ and $FeCl_4^-$. The λ-$GaCl_4$ salt is an ambient-pressure superconductor with T_c=8 K, while the λ-$FeCl_4$ salt exhibits very sharp metal-insulator transition at the same temperature. The crystal structures are very similar to each other. An important difference lies at the counter anion; the Fe^{3+} ion is magnetic unlike the diamagnetic Ga^{3+} ion. The ESR measurement indicates that the Fe^{3+} ion is in the high-spin state and the metal-insulator transition in the λ-$FeCl_4$ salt is accompanied by an anti-ferromagnetic ordering of the Fe^{3+} moments. The application of magnetic fields $\geqslant$10 T suppresses the sharp metal-insulator transition [49]. It is proposed that this unusual phenomenon (a field-restored highly conducting state; FRHCS) is

connected to ferromagnetic ordering of the Fe^{3+} moments under the high magnetic field.

2. Structural Changes and Electronic Properties

Organic conductors frequently undergo a change in electronic properties accompanied by a structural change with varying temperature or pressure or both. This is predominantly due to the system's low-dimensional nature which enhances the electron–lattice or spin–lattice interaction to cause dramatic changes in electronic and structural properties. Among them the most typical phase changes are the Peierls and the spin-Peierls transitions that were first found and studied in detail in molecular conductors.

2.1. Peierls transition

In the middle 1970s metallic nature and the transition into the insulating state were found in two molecular systems, KCP ($K_2Pt(CN)_4Br_{0.30}3.2\ H_2O$) and TTF–TCNQ (tetrathiafulvalene-tetracyanoquinodimethane), both of which have highly one-dimensional electronic systems [50,51]. These behaviors were different from those having been found in other molecular conductors in two points; a lot of unquestionable experimental evidences for the metallic properties, and a clear structural change accompanying the metal-insulator transition. The origin of the transition was clarified to be the Peierls transition, which will be discussed below. The discovery of the Peierls transition in KCP and TTF–TCNQ were followed by those in organic conductors such as TSeF–TCNQ, HMTTF–TCNQ, HMTSF–TCNQ, NMP–TCNQ, TMTSF–DMTCNQ [51], and in inorganic conductors like TaS_3, $NbSe_3$, $K_{0.3}MoO_3$, $(TaSe_4)_3I$ and $(NbSe_4)_3I$ [52]. In the following we shall focus on TTF–TCNQ as a good example for the discussion of structure–property relationship.

Figures 13 and 14 show the crystal structure and the temperature dependence of electrical conductivity measured along the one-dimensional axis, *b*-axis, of TTF–TCNQ [53]. The conductivity increases with decreasing temperature down to about 60 K below which the conductivity is characterized by thermally activated nature. The metallic properties are ascertained by much experimental evidence such as optical reflectivity, spin-magnetic susceptibility, and thermopower [54]. In the insulating state similar measurements also suggest the presence of a band gap at the Fermi level. These measurements suggest the metal-insulator transition to occur at 53 K.

Diffuse X-ray and elastic neutron scattering studies revealed the presence of a structural change accompanying the metal-insulator transition: In the insulating state below 53 K a set of satellite reflections was discovered with the superlattice

period $b' = 3.4\ b$ [55,56]. The superstructure is found to be formed by the sinusoidal molecular displacement having the wave vector whose *b*-component $Q_b = 0.295\ b^* = (1/3.4)\ b^*$. Figure 15 shows the temperature dependence of the intensity of the superlattice reflection, which is approximately proportional to the square of the displacement amplitude [55–57].

This type of metal-insulator transition is considered to be nothing but the Peierls transition that had been proposed by R.E. Peierls to explain the electronic properties of bismuth [58]. He pointed out that a one-dimensional metal is unstable at low temperatures to undergo a metal-insulator transition accompanied by charge-density waves (CDW). A precursor phenomenon of the Peierls

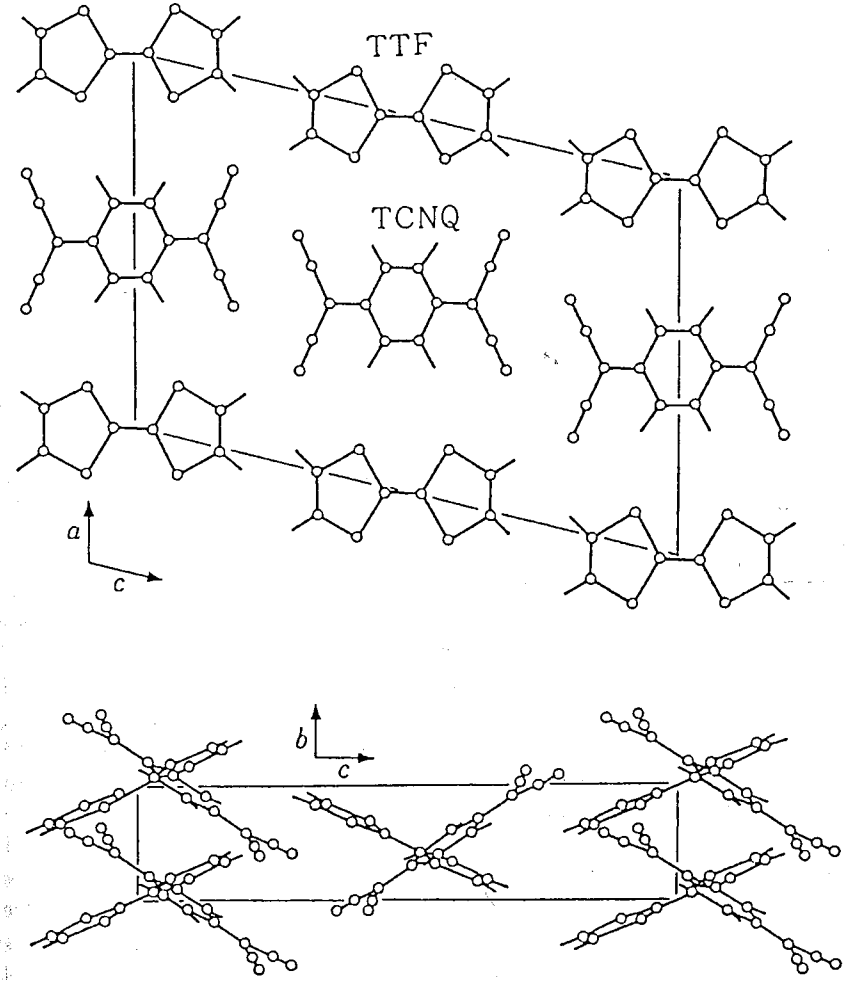

Figure 13 Crystal structure of TTF–TCNQ

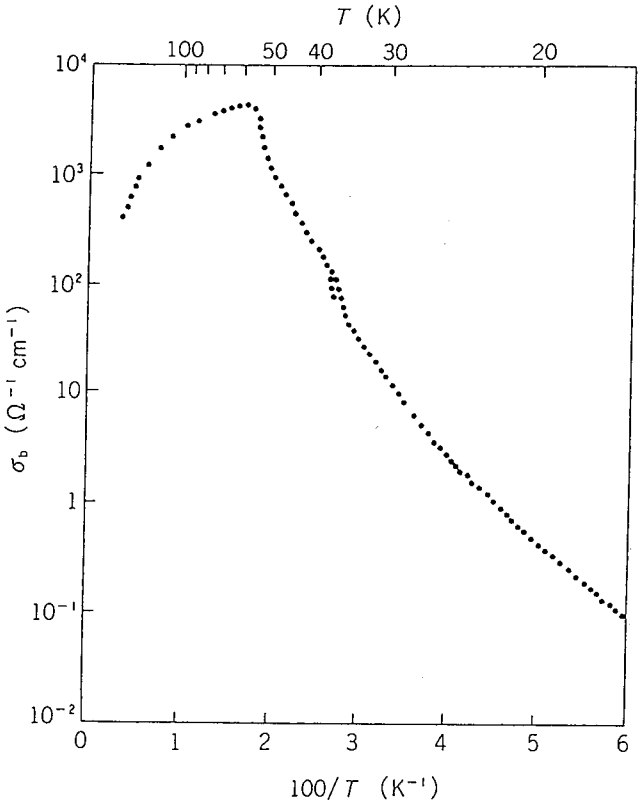

Figure 14 Temperature dependence of the dc electrical conductivity of TTF–TCNQ. (Reproduced from T. Ishiguro et al., J. Phys. Soc. Jpn., 41 (1976) 351, Fig. 1(a))

transition is the phonon softening due to the electron-phonon interaction with the wave number $2k_F$. It is called the Kohn anomaly [59].

The mechanisms of the Peierls transition is explained intuitively as the following: Figure 16(a) depicts a one-dimensional metallic conduction band occupied up to the Fermi potential E_F and the Fermi wave number k_F. When one introduces a periodic potential due to the molecular displacement having the period of $2\pi/2k_F$, the size of a unit cell is enlarged to $2\pi/2k_F$ in which two electrons reside occupying the lowest energy level. In the momentum space the reciprocal lattice has the size of $2k_F$. Therefore, according to elementary solid state physics, a band gap opens at $k=k_F$ and $-k_F$ where the electron energy $E=E_F$ as shown in Fig. 16(b). This situation is nothing but that of a band insulator or an intrinsic semiconductor. In one-dimension this mechanism occurs automatically because of the energy gain by the amount of the gap energy.

The Peierls transition is described in terms of the "polarization function" (or the "density-response function") $\chi(q)$: For the potential $V(r)=V_q \cos qr$ a metallic

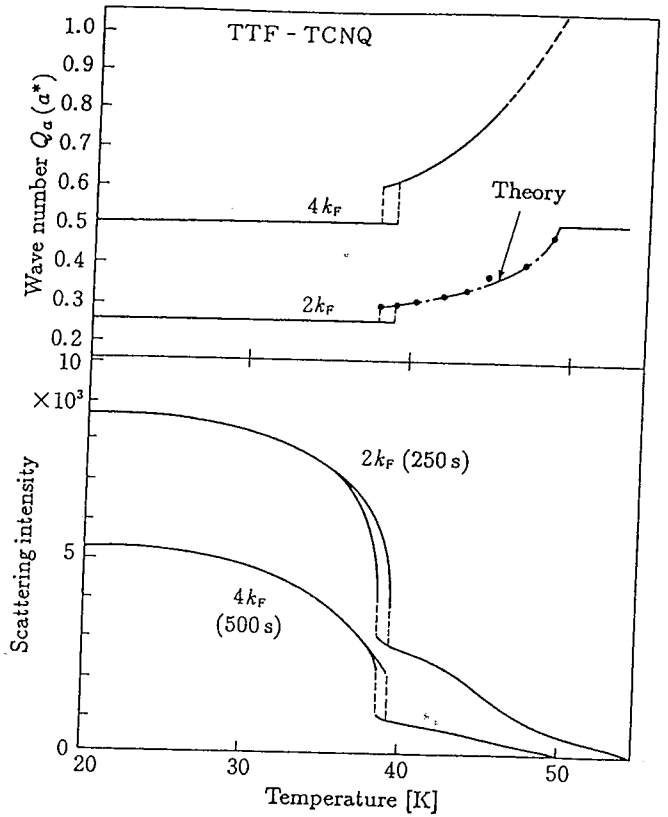

Figure 15 Temperature dependence of the intensity and the transverse wave number of the $2k_F$ and the $4k_F$ X-ray satellite reflections in TTF–TCNQ. (Reproduced from S. Kagoshima et al., J. Phys. Soc. Jpn., 41 (1976) 2061, Fig. 9)

electron system causes the density response $\rho(r)=\rho_q \cos qr$. In the lowest order approximation one expects the linear relation

$$\rho_q = -V_q \chi(q).$$

The first order perturbation calculation gives

$$\chi(q)=\frac{1}{N}\sum_k \frac{f(E_{k+q})-f(E_k)}{E_k - E_{k+q}}$$

where $f(E_k)$ denotes the Fermi distribution function for the electron having the wave number k and the energy E_k, and N is the number of electrons. Figure 17 shows the q-dependence of $\chi(q)$ at $T=0$. In one-dimension $\chi(q)$ shows a logarithmic divergence for $q=2k_F$. Temperature dependence of $f(E_k)$ dominates that of $\chi(q)$ giving also the logarithmic divergence for $T\to 0$ at $q=2k_F$. This leads to the onset of the finite amplitude of electronic density wave of $q=2k_F$ with

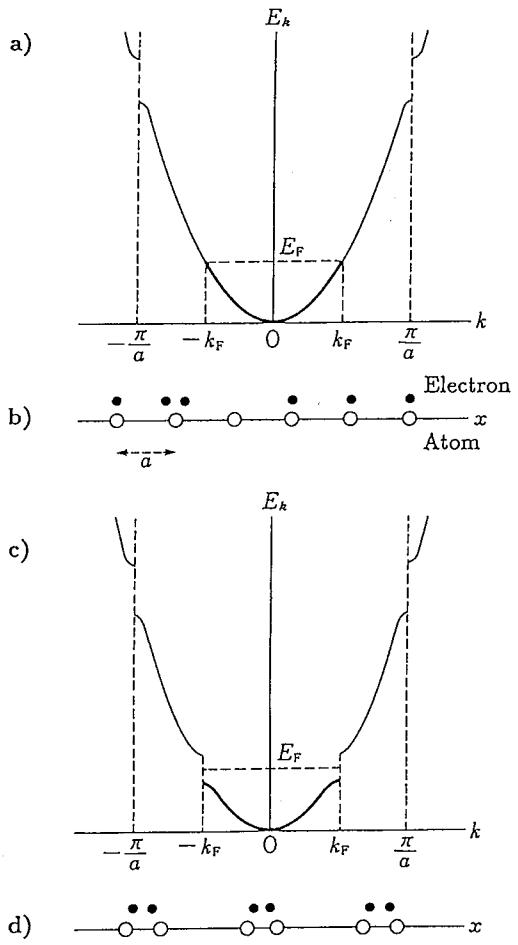

Figure 16 A band picture and a classical particle one for the Peierls transition. (a) metallic band, (b) particle picture of metal, (c) band with the Peierls gap, (d) particle picture of the insulating state for the electron density $n = 1/a$.

decreasing temperature for an arbitrarily small potential amplitude V_q. This suggests a strong electron–phonon interaction for the wave number $q = 2k_F$.

In the metallic state below about 150 K a set of diffuse streaks was found in X-ray studies as shown in Fig. 18 which suggests the onset of the periodic lattice distortion with $Q_b = 0.295\ b^*$ having no correlation among them perpendicular to the one-dimensional b-axis [55,56]. Corresponding to these x-ray streaks inelastic neutron scattering studies revealed the decrease in the phonon frequency for the wave vector $Q_b = 0.295\ b^*$ with decreasing temperature as shown in Fig. 19 [60]. This soft phonon is considered to be frozen out at the metal-insulator transition temperature 53 K causing the superstructure described above. This type

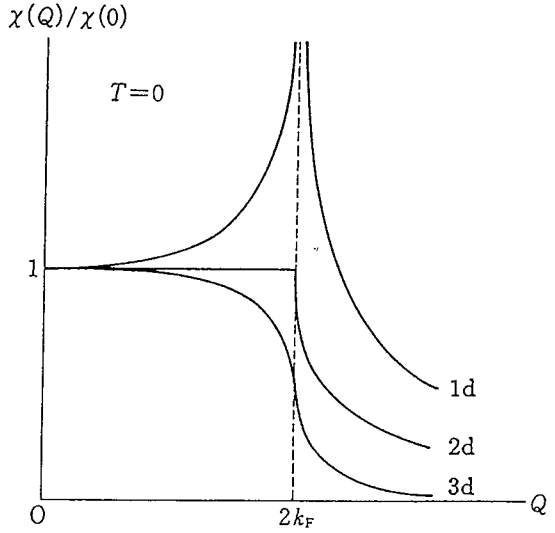

Figure 17 Wave number dependence of the polarization function in each dimension.

of phonon softening is called the "giant Kohn anomaly" due to the strong electron–phonon interaction with the wave number $2k_F$. It causes the renormalization of the phonon frequency Ω_q,

$$\Omega_q^2 = \omega_q^2 - \frac{2|g_q|^2\omega_q N}{\hbar V}\chi(q)$$

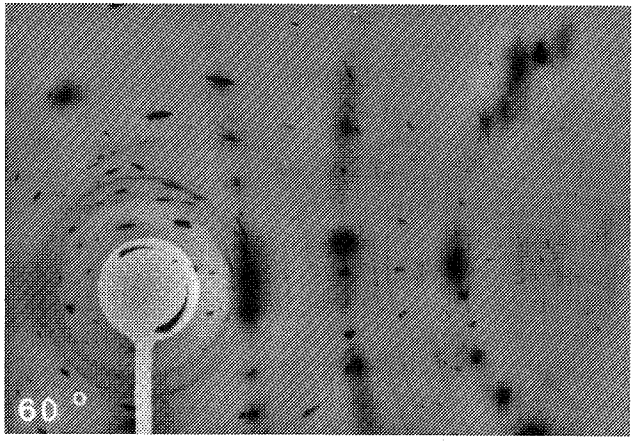

Figure 18 X-ray monochromatic Laue pattern of TTF–TCNQ at 110 K. The horizontal direction is parallel to the one-dimensional b-axis. (Reproduced from J. P. Pouget et al., Phys. Rev. Letters, 37 (1976) 437, Fig. 1(a))

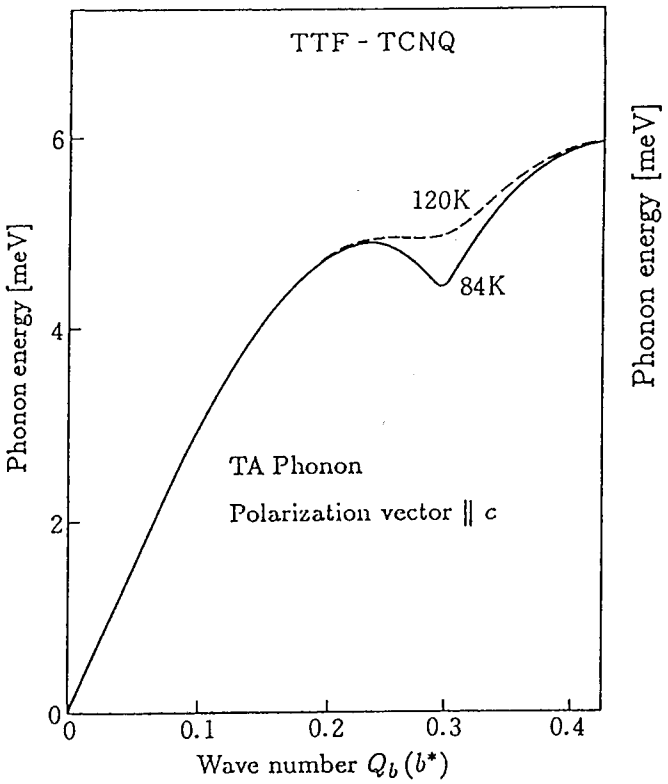

Figure 19 Kohn anomaly observed by inelastic neutron scattering.

where ω_q and g_q denote the bare phonon frequency and the electron–phonon interaction parameter, respectively, and V is the system volume. The divergence of $\chi(q)$ for $q=2k_F$ and $T\rightarrow 0$ causes the giant Kohn anomaly. The Peierls transition is considered to occur at the temperature T_P where $\Omega_q=0$. Below T_P the lattice distortion with $2k_F$ is frozen out leading to the onset of a mixed wave of the periodic lattice distortion and the electronic density wave. It is called a charge-density wave (CDW). Usually X-ray and the neutron scatterings probe the lattice component of CDW.

The Peierls transition and the giant Kohn anomaly are driven by the divergence of the polarization function $\chi(q)$ for $q=2k_F$. Conditions for the divergence are understood intuitively in terms of the "nesting" of the Fermi surface: Figure 20 shows the three dimensional representation of the Fermi surfaces of one- and two-dimensional electron systems. The divergence of $\chi(q)$ at T=0 is considered to be ascribed to the condition, $E_{k+q}-E_k=0$ and $f(E_k)-f(E_k+q)\neq 0$. It is satisfied for k on the Fermi surface (solid curve) which lies also on the Fermi surface (broken curve) shifted by q. In one-dimension all k-states on the Fermi surface contribute to the divergence for $q=2k_F$. In two-dimension any q less than

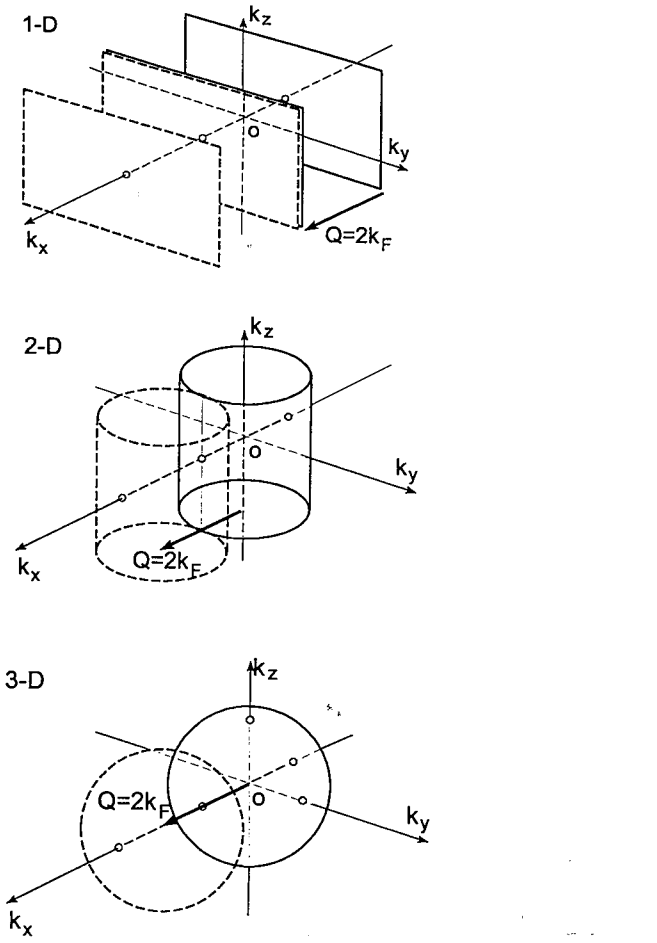

Figure 20 Three-dimensional representation of the Fermi surfaces and their nestings in each dimension.

$2k_F$ makes only the k-states on the two lines shown in the figure satisfy the divergence condition. A contact between the original Fermi surface and the shifted one, the "nesting", dominates the divergence of $\chi(q)$. The nesting is perfect in one-dimension.

Applying the concept of the Peierls transition to TTF–TCNQ $2k_F$ is evaluated as 0.295 b^*. It leads to the band filling up to 29.5% of the first Brillouin zone. The average valences of TTF and TCNQ are expected as +0.59 and −0.59, respectively. This is verified by X-ray photoelectron spectroscopy (XPS) [61]. The upper panel of Fig. 15 shows temperature dependence of the transverse component of the wave vector $\boldsymbol{Q}$ of CDW. Generally the transverse components

of CDW's wave vector are dominated by the good nesting condition for the Fermi surface. In many CDW systems, however, they are explained in terms of the interchain interaction between CDW on each molecular stack. In TTF–TCNQ the interchain Coulomb interaction energy is minimized by the phase difference of π between two neighboring CDW, $\rho_0 \cos Qx$ and $\rho_0 \cos (Qx+\pi)$, leading to the two-fold superstructure parallel to the c-axis, $Q_c = 0.5c^*$. This has also explained Q_a in the range 53 K–49 K because CDW is considered to develop only on the TCNQ stacks. The successive transition in Q_a in the range 49 K–38 K is explained by taking account of the onset of another CDW on the TTF stacks below 49 K [62].

CDW can bear an electric current while the system is insulating below T_P in the sense of the single particle transport. The current is carried by a CDW sliding in the lattice with no restoring force at $T=0$ if $2k_F$ is incommensurate with the underlying reciprocal lattice. In real materials impurities or lattice defects interact with the CDW leading to various phenomena such as the nonlinear transport, a type of mode-locking etc. [63] However, we will leave these problems out of the scope of this article.

Transport, magnetic and structural studies of the metal-insulator transition in the quasi-one-dimensional conductor $(TMTSF)_2PF_6$ verified that the transition is accompanied by the onset of spin-density waves (SDW) without any structural change [64]. When the electron–electron Coulomb interaction is large, the good nesting of the Fermi surface is expected to give the SDW instead of CDW. A naive picture of SDW is given as purely electronic density waves of up- and down-spins adjusting their phase difference to π to lower the exchange interaction energy between them. Its wave-length is just the same as CDW. The system becomes an insulator as for CDW because the up-spin electrons give a $2k_F$ potential of magnetic origin to the down-spin ones and vice versa. Magnetically the system is nothing but an anti-ferromagnet. It is to be noted that the magnitude of magnetic moment on each molecule is usually a fraction of the Bohr magneton μ_B because of the band origin.

Recently the coexistence of the $2k_F$ CDW with SDW has been found by a diffuse X-ray scattering study of $(TMTSF)_2PF_6$ [65]. This has been ascribed to a purely electronic CDW involving no lattice distortion. In the conventional model of SDW the charge density should be uniform. Very recently a theory has succeeded to explain the coexistence of the purely electronic $2k_F$ CDW with SDW in terms of the next-nearest-neighbor Coulomb interaction between electrons [66]. It is interesting to find the coexistence also in other materails.

2.2. $4k_F$ structure

The band model employed in the last section did not take account of the Coulomb interaction energy between conduction electrons $V(r)$ where r denotes the distance between two electrons. The long-range Coulomb interaction like

$V(r) \sim 1/r$ makes two electrons apart from each other. This Coulomb energy competes with the kinetic energy of electrons. Therefore, the ratio V/W is a key parameter to discuss the electronic properties, where V denotes the order of magnitude of the Coulomb interaction evaluated for, for example, $r \sim$ the molecular size.

For $V/W \gg 1$ electrons are localized and the metallic conduction is forbidden. The electrons will form a "crystal" in which they are arranged with equal distance. This is called the Wigner crystal. In one-dimension the distance between neighboring electrons is given as $1/4k_F$ because the distance is $1/n$ and $k_F = \pi n/2$.

In the diffuse X-ray measurements of TTF–TCNQ the superlattice reflection was found with the wave number $4k_F = 0.59\ b^*$ [56]. It is observed even at room temperature and suggests the absence of the interchain correlation above 49 K. A set of superlattice reflection was found below 49 K suggesting the formation of an ordered structure of three-dimension. This superstructure is ascribed to the molecular displacement caused by the Wigner crystal of electrons through the electron-lattice interaction [67]. The $4k_F$ structure is considered to be formed predominantly on the TTF stacks. The $2k_F$ superstructure is rather ascribed to TCNQ stacks. This is suggested [68] by detailed analyses of the results of X-ray, neutron, EPR and NMR measurements.

When the long-range Coulomb interaction is small, one can take account of only the on-site Coulomb interaction energy U between two electrons on a molecule. This electronic system is described in terms of the Hubbard model. Theoretical studies have shown that for $U/W \gg 1$ the electrons undergo the Mott transition which does not necessarily involve any structural changes. The electrons are localized with equal distance. They are apparently the same as the Wigner crystal described above. It is shown that the Mott transition is easy to occur when the charge density is 1/molecule or 1/site.

2.3. Spin Peierls transition

When the strong Coulomb repulsion works between electrons, the electrons are regarded as localized particles. In one-dimension the localized spins can undergo a magnetic transition either to an anti-ferromagnetic state or a Spin Peierls state that has no spin [69].

Figure 21 shows temperature dependence of electrical conductivity and magnetic susceptibility of MEM(*N*-methyl-*N*-ethyl-morpholinium)-$(TCNQ)_2$ [70]. At about 335 K it undergoes a metal-insulator transition accompanied by the onset of a two-fold superstructure and a temperature dependent magnetic susceptibility characteristic of localized moments. It is considered as depicted in Fig. 22(a) that a dimerized TCNQ accepts an electron localized by, for example, the Mott transition or the Wigner crystallization. The solid curve shown in Fig. 21(b) denotes the theoretical prediction for the magnetic susceptibility of a one-

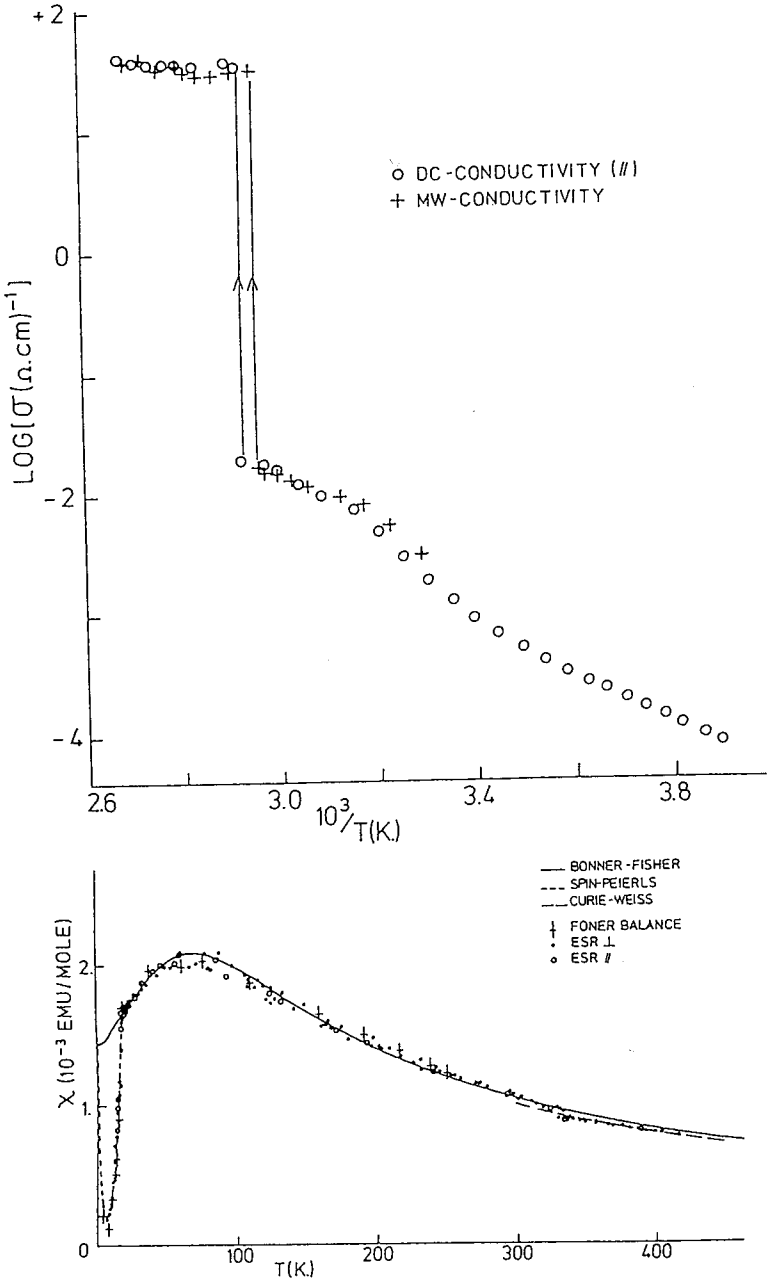

Figure 21 Temperature dependence of the dc electrical conductivity and the static magnetic susceptibility of MEM-$(TCNQ)_2$. (Reproduced from S. Huizinga et al., *Quasi One-Dimensional Conductors II* ed. S. Barisic et al., (Springer, Berlin, 1979) p. 45. Figs. 7 and 8)

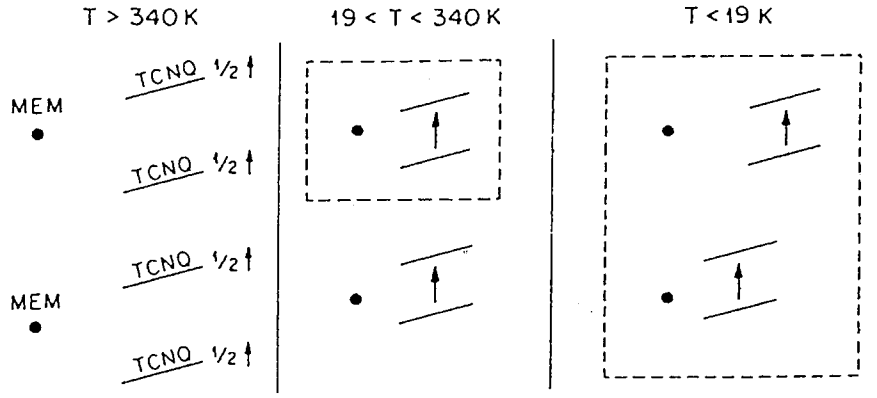

Figure 22 Schematic view of the metallic ($T>340$ K), $4k_F$ charge-localized ($19<T<340$ K) and the $2k_F$ spin-Peierls ($T<19$ K) states of MEM–$TCNQ_2$.

dimensional chain of Heisenberg spins whose spatial positions are fixed. This is called the Bonner–Fisher type susceptibility [71]. Below 19 K, however, the magnetic susceptibility decreases rapidly with decreasing temperature while the electrical resistance shows no specific change. Structural measurements verified the onset of a four-fold superstructure below this temperature [72]. This suggests two localized electrons form a pair whose total spin is zero as depicted in Fig. 22. This magnetic transition involving the lattice distortion is called the spin Peierls transition. The three-dimensional nature of a real system can lead to another state, an anti-ferromagnetic state, depending on the magnitude of the interchain interaction [73]. Problems of the spin Peierls transition have been studied in detail also in other materials such as TTF–$MX_4C_4(CF_3)_4$ [69].

When magnitude of the electron-electron Coulomb interaction increases, the system is expected to show a change from the SDW dominated state to the spin-Peierls one. This was verified in another system, (TMTTF(tetramethyltetrathiafulvalene))$_2$X and $(TMTSF)_2X$ [74]. The former materials have the narrower band width than the latter. This means that the role of Coulomb interaction is more important in the former system than in the latter. The former system is expected to have the spin-Peierls state and the latter one the SDW state. Systematic studies have proposed the phase diagram shown in Fig. 23 [74].

2.4. *Anion ordering*

The preceding three sections described the structural changes whose driving force is the low dimensional nature of the electron system. Sometimes structural changes occur rather independent of electronic properties. One of such examples is the anion ordering transition observed in $(TMTSF)_2ClO_4$.

The anion ClO_4 is located at the center of inversion symmetry in the crystal of $(TMTSF)_2ClO_4$ although the anion itself has the tetragonal shape with no

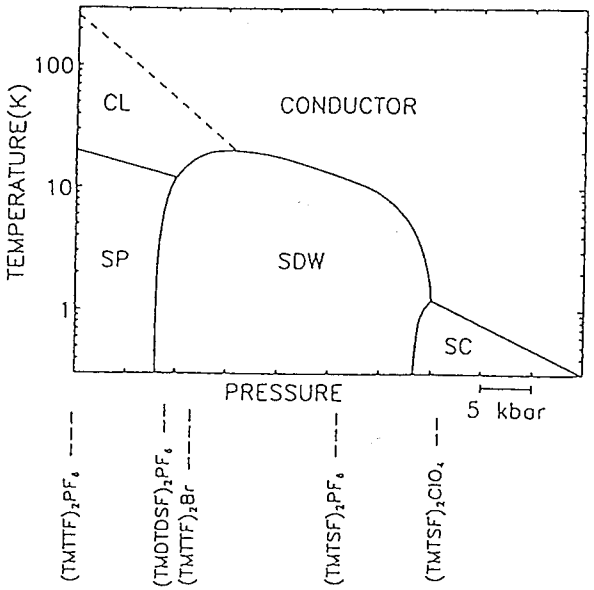

Figure 23 Schematic phase diagram of the (TMTTF, TMTSF)$_2$X system. (Reproduced from D. Jerome, Organic Conductors, Ed. J-P. Farge (Marcel Dekker, 1994) p. 420, Fig. 5)

inversion symmetry. Under this circumstance the anions can undergo an orientational ordering through the anion–anion interaction presumably via TMTSF molecules.

Diffuse X-ray studies revealed the onset of a superstructure in (TMTSF)$_2$ClO$_4$ due to the ordering of ClO$_4$ at about 24 K [75]. Figure 24 shows schematically the ordering pattern of ClO$_4$ in the unit cell [76]. The unit cell is doubled along the *b*-axis. It was found that the ordering transition took a rather long time to complete. The ordering becomes imperfect if the sample is quenched in the range 30 K–20 K with the speed of the order of 1 K/min or faster [77]. It had been experienced that the sample had to be slowly cooled to realize the superconductivity. Otherwise the spin-density wave appeared. The finding of the

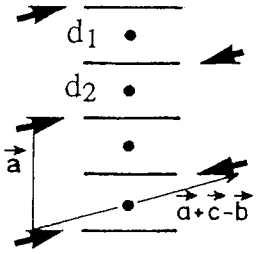

Figure 24 Schematic view of the orientational ordering of ClO$_4$ in (TMTSF)$_2$ClO$_4$.

quenching effect in the structural change gives a direct explanation for these phenomena: the imperfect ordering of ClO$_4$ suppressed the onset of the superconductivity.

The relation between the orientational ordering and the onset of the superconductivity or the spin-density wave is conjectured as the following: The orientational ordering is expected to cause first the reduction of the lattice parameter presumably due to the orientational ordering of the non-spherical anion, and second the re-construction of the Brillouin zone because of the unit-cell doubling along the *b*-axis. The first effect is really verified by the lattice parameter measurements [78]. The reduction in the intermolecular distance along the *b*-axis is expected to increase the conduction bandwidth along this direction. It will lead to the suppression of the Fermi surface nesting because of the increase in the degree of warping of the quasi one-dimensional Fermi surface. This will suppress the spin-density wave and lead to the superconductivity. The second effect gives the two-fold Fermi surface in the re-constructed first Brillouin zone. Also for this case the nesting is expected to be suppressed because of the presence of many nesting vectors. When a sample is quenched, the spin-density wave appears below about 6 K. The disorder due to the quenching seems to give little effect to the onset of the spin-density waves.

The orientational ordering has also been found in other TMTSF compounds having asymmetric anions, such as ReO$_4$, NO$_3$, FSO$_3$ [76]. In these materials the one-dimensional axis, *a*-axis is doubled by the orientational ordering. Therefore the anion ordering causes a metal-insulator transition because the band gap at the Brillouin zone boundary opens just at the Fermi level.

2.5. *Interplay among various mechanisms*

The quasi one-dimensional molecular conductor (R$_1$R$_2$DCNQI)$_2$Cu shows novel electronic properties discussed in the last section. With increasing pressure the metallic state becomes unstable undergoing a metal-insulator transition. In addition the system undergoes a metal-insulator-metal re-entrant transition with lowering temperature in a narrow pressure range above a critical pressure of about 0.1–0.5 kbar (10–50 MPa) [79].

Extensive studies have revealed the mechanism for these novel properties. It is the interplay among many mechanisms; the Peierls instability characteristic of one-dimensional system, the Mott transition in Coulomb interacting system, the mixed valence of Cu, the Jahn-Teller effect of Cu^{2+} ions, and the Curie-Weiss paramagnetism of the 1/2-spin of Cu^{2+}. The key role in showing the variety of properties was played by the structural deformation which causes a shift in the energy level of d-electrons of Cu.

The d-like band is partially filled up to 5/6. The π-like band is occupied up to 1/3. The Peierls instability in the quasi one-dimensional π-like band causes a superstructure with the period of 3*c*. This reduces the first Brillouin zone to 1/3

of the original. The uppermost d-like band becomes just half filled and, according to a general rule of the Mott transition, is unstable for the Mott transition leading to a charge ordering with the period of $3c$. Thus the two mechanism, the Mott transition and the Peierls one cooperate to make the system insulating with the superstructure of $3c$.

The above scenario for the metal-insulator transition is verified by X-ray diffraction studies: In the high temperature regime of metallic state the N–Cu–N bond angle α was found to increase with decreasing temperature [80]. This suggests an up-shift of the uppermost d-level of Cu as experienced in the Jahn–Teller effect. This is expected to increase the quantity of Cu^{2+} leading to the increase of the average valence toward +4/3, which is preferable to the metal-insulator transition discussed above.

In the insulating state a three-fold superstructure is found by X-ray measurements as shown in Fig. 25 [81]. Also a step-wise increase in the angle α is found at the transition temperature [80,82]. This suggests that the metal-insulator transition with increasing pressure or decreasing temperature is triggered by the increase of the one-dimensionality that stimulates both the Mott and the Peierls transitions [83]. The increase in the transition temperature with increasing pressure suggests the more compression of the c-axis than the a. It is consistent with the larger thermal contraction in the c-axis.

In the re-entrant transition from the insulating to the metallic state with decreasing temperature just the restoration to the metallic state has been found in electrical, magnetic and structural properties. It is not surprising to have the re-entrant transition because of the free energy of the system. The metallic state's free energy is expected to be proportional to $-T^2$ because of the electronic heat

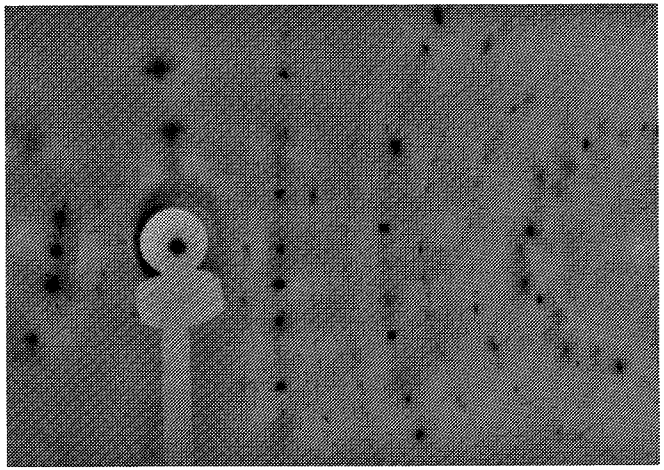

Figure 25 X-ray monochromatic Laue pattern of (MeCl–DCNQI)$_2$Cu at about 20 K. The horizontal direction is parallel to the one-dimensional c-axis. (Reproduced from R. Moret, Synth. Met. 27 (1988) B301, Fig. 1 (B))

capacity while that of the insulating state $-T$ due to the entropy of paramagnetic spins. The metallic state can have the lower free energy if the pre-factor of each energy term satisfies a certain condition [84].

3. Theoretical Overview

3.1. Introduction

As has been introduced in Sections 1 and 2 of this chapter and in other Chapters, the variety of electronic properties of molecular solid can have and so far have been realized is very broad. This is another manifestation of the unpredictable possibility materials around us can have. While it is important and decisive for the future development to pursue such a diversity based on the experimental studies on each system, the search for systematics of material properties on the theoretical ground is necessary for the establishment of new concepts, which will in turn be transferred back to the experimental activities. This section is intended to review recent theoretical studies aiming at possible classifications and constructions of unifying view on these materials.

The theoretical considerations are based on the fact that in these molecular crystals the molecular orbitals are good basis for the descriptions of low energy excitations. Actually the extended Hückel type of the tight-binding approximation for the band structure calculations based on these molecular orbitals work very well as has been confirmed by the angular dependent magnetoresistance (AMR) (see Section 1). Moreover it is to be noted that the results of the recent first principle band structure calculations on (DCNQI)$_2$Cu [85] agree with the de Haas–van Alphen experiment [86]. Such extended Hückel approximations, however, fail in cases where some kinds of phase transition occur and the ground state are no longer normal but has some kind of long range order. Such states include the Peierls or spin Peierls (SP) state, antiferromagnetism including spin density wave (SDW) and superconductivity (SC). The causes of such long range orders are the electron–phonon interaction and the mutual Coulomb interactions between electrons, the former of which is now well known to lead to the Peierls state with charge density wave (CDW).

In the following the review is given on the theoretical studies on the effects of mutual Coulomb interactions under the assumption that the electronic state at each site is properly represented by one molecular orbital. Then the Hamiltonian will be expressed as follows,

$$H=\sum_{i,j} t_{ij}a_{is}^{+}a_{js}+U\sum_{i} n_{i\uparrow}n_{i\downarrow}+\frac{1}{2}\sum_{i,j} V_{ij}n_i n_j .$$

Here t_{ij} is the transfer integrals between molecules, i and j, and U and V_{ij} are on-site and intersite Coulomb interactions, respectively, and $n_{is}=a_{is}^{+}a_{is}$ and

$n_i = n_{i\uparrow} + n_{i\downarrow}$. In the actual treatment of the Coulomb interactions the Hartree-Fock (HF) approximation will be employed, where U and V_{ij} terms are approximated as follows,

$$Un_{i\uparrow}\langle n_{i\downarrow}\rangle \rightarrow Un_i\langle n_{i\uparrow\downarrow}\rangle + Un_{i\downarrow}\langle n_{i\uparrow}\rangle - U\langle n_{i\uparrow}\langle n_{i\downarrow}\rangle,$$

$$V_{ij}n_i n_j \rightarrow V_{ij}n_i\langle n_j\rangle + V_{ij}n_j\langle n_i\rangle - V_{ij}\langle n_i\rangle\langle n_j\rangle.$$

This HF approximation is the durable and systematic procedures for the search of the possible ground states. (The above approximation to the V_{ij} term is the Hartree approximation, but we use the term HF below for simplicity.) It should be kept in mind, however, that the quantitative aspects of results of this approximation should not be taken literally but that the results will be a basis for the further detailed theoretical studies.

3.2. *Various ground states so far realized in organic crystals*

3.2.1. Peierls state

This is the state that has been first realized in TTF–TCNQ and triggered the scientific activity toward the molecular crystals [87]. Due to the electron–phonon interaction and strong nesting of the one-dimensionality of the π-band, the original lattice gets unstable toward to the formation of the superlattice with the periodicity of $2k_F$, k_F being the Fermi momentum [88]. In this state the CDW with same wave vector, $2k_F$, is established and the energy gap is created at the Fermi energy of electrons as in ordinary insulators and then spin susceptibility, χ, is suppressed: i.e. the Peierls state is non-magnetic. The conductivity at low frequencies, however, survives because of the sliding degree of freedom of the phase of CDW, i.e. phasons, especially if $2k_F$ is incommensurate with the reciprocal lattice vector [89]. In the static limit, however, the conductivity vanishes because of the pinning of CDW by impurities [90]. The commensurability also acts as a pinning mechanism.

3.2.2. SDW state

This state, which has a spatially periodic magnetization with wavevector, $2k_F$, is realized in the presence of high degree of the nesting of the Fermi surface on one hand and the short-ranged repulsive interactions between electrons on the other [91]. The magnetic properties of this state is essentially the same as those of Néel state, but with smaller amount of the magnetization, while the transport properties are in general similar to those of CDW state, i.e. insulating.

3.2.3. Superconducting (SC) state

Because of the limited dimensionality and anisotropy of the systems, the symmetry of SC order parameters is not always the same as that of BCS but can be anisotropic with line nodes [92].

3.2.4. Charge disproportionation (CD) or charge ordering (CO)

The metallic states in molecular crystals are realized first of all by the charge transfer (CT) between segregated donors and acceptors. The actual conduction can be along either donors or acceptors: in the case of ET_2X, e.g. on ET donors. In the presence of several inequivalent sites in a unit cell, some site(s) can have a different amount of carrier density from the other site(s), which is termed as CD, or CO.

3.2.5. Mott insulators

In the presence of strong on-site Coulomb repulsive interaction, U, (compared with the kinetic energy typically represented by the band width, W) at half filling in non-degenerate band, i.e. if the total number of electrons, N_e, is equal to the total number of lattice sites, N, electrons are localized at each lattice site to avoid the Coulomb repulsion. This is the Mott insulator. In this state one Bohr magneton of spin is present in each site to start with as shown in Fig. 26. Such a case quite often results in magnetically ordered state, e.g. Néel ordered state, because of the superexchange interactions, J, between spins. Such magnetic interaction processes, which govern the low energy excitations, are properly described by the Heisenberg spin model. Note that in this Mott insulator the charge excitations are pushed up to the region of the very high energy (of the order of U). Hence spin and charge are separated in the Mott insulators in the low energy region. This is called the spin-charge separation.

3.2.6. Wigner solid (WS)

In non-degenerate narrow bands the screening of Coulomb interaction is not necessarily strong and then the longer ranged part of the Coulomb interaction, V_{ij}, could in principle play important roles besides the on-site Coulomb interaction, U. Typically those between the neighboring sites, V, play particular roles at quarter filling as is easily understood as in Fig. 27. This state can be considered as a kind of CO state and is called the Wigner solid especially when the electrons are localized in regular interval.

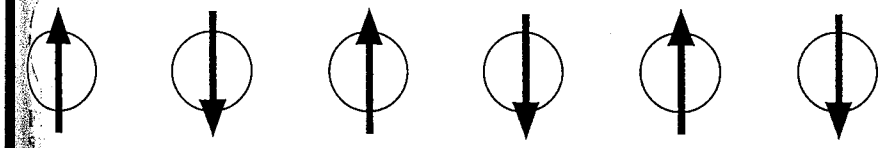

Figure 26 A schematic view of the Mott insulating state. Circles and arrows represent sites and electron spins, respectively.

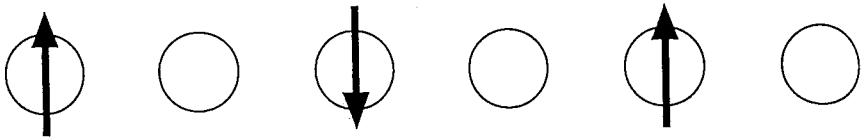

Figure 27 A schematic view of the WS state.

3.2.7. *Antiferromagnetic Néel (AF) state*

Since the superexchange interaction, J, in the Mott insulators with non-degenerate orbitals is antiferromagnetic between neighboring sites, the Néel state is usually the ground state with magnetic moment close to one Bohr magneton on each site with possible reductions due to the quantum fluctuations intrinsic to low dimensionality. The magnetic frustrations also cause such reduction of spins, and in some cases, total destruction of the magnetic moments.

3.2.8. *Spin-gapped (SG) state*

Even in the Mott insulators, where localized spins are present at each site, non-magnetic ground states are sometimes realized where the spin susceptibility is vanishing toward absolute zero. An example is the formation of the singlet state realized by the dimerizations. The frustration can also lead to the non-magnetic ground state.

3.2.9. *Spin-Peierls (SP) state*

In some of quasi one dimensional antiferromagnetic Heisenberg systems with spin $S = 1/2$, the non-magnetic singlet ground state is realized by the alternating superexchange interaction caused through the dimerizations of lattice as in the Peierls state, as schematically shown in Fig. 28. This dimerized state, which is called the spin-Peierls state, is theoretically described as the Peiels state of spinless fermions introduced by the Jordan-Wigner transformation of spins [93].

In the following, theoretical discussions are made on each case of typical examples of organic conductors so far studied in detail.

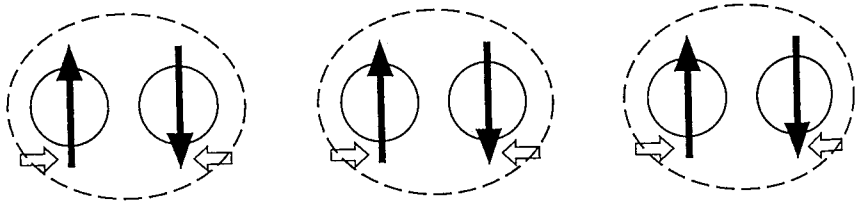

Figure 28 A schematic view of the SP state. The white arrows show the lattice distortion.

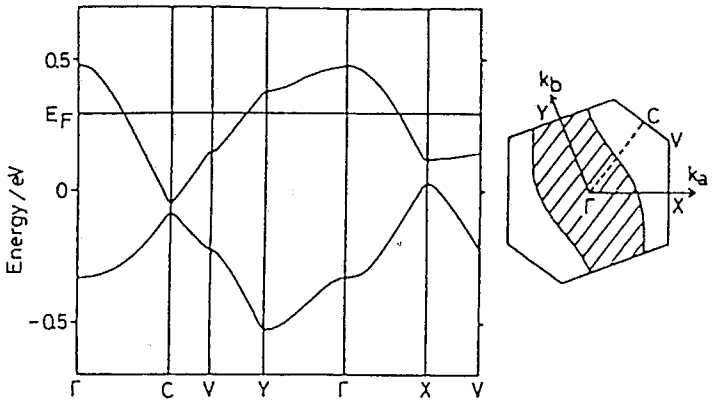

Figure 29 Band structure and Fermi surface of $(TMTTF)_2X$ calculated within the extended Huckel approximation. (taken from ref. 10)

3.3. *$(TMTCF)_2X$*

TMTCF denotes TMTTF or TMTSF molecule. The amount of charge transfer in this family with one-dimensional structures is such $TMTCF^{1/2+}$ and X^{1-}. The band structure and the Fermi surface are open as shown in Fig. 29 for the case of $(TMTTF)_2X$ [94]. The phase diagram of this family on the plane of pressure (p) and temperature (T) is shown in Fig. 30 proposed by Jérome [95]. The major

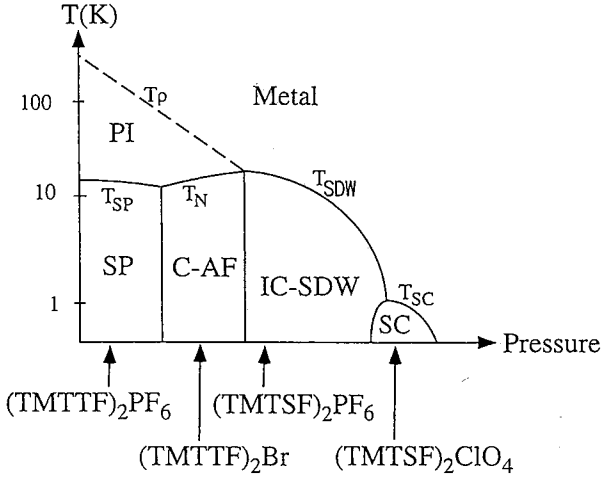

Figure 30 Phase diagram of $(TMTCF)_2X$ proposed by Jerome [95]. PI, SP, C-AF, IC-SDW and SC represent paramagnetic insulating, spin-Peierls, commensurate antiferromagnetic, incommensurate spin density wave and superconducting phases, respectively. T_ρ denotes the temperature where the resistivity shows the minimum.

effects of pressure in this case are considered to be the increase of the interchain transfer integrals resulting in the more warping of the Fermi surfaces on one hand and the reduction of the effective strength of Coulomb interaction on the other. In order to understand the overall features of this phase diagram, it is to be noted that, as seen from Fig. 29, the band is half filled instead of the quarter-filling which is expected if all TMTCFs are equivalent. This half-filling is due to the existence of the weak dimerization due to the alternation of the transfer integrals along the chain direction. However it is to be noted that this dimerization is very weak compared with the mutual Coulomb interactions as will be easily inferred by the smallness of the band-gap seen in Fig. 29, and then half-fillingness of this system should be taken with care. Actually the origin of the insulating state in the region of low pressure will be the WS driven by the intersite Coulomb interaction, V [96], rather than the Mott insulators expected for case with one carrier per site. Once carriers (holes in this case) get localized and the system is insulating, and then there exist localized spins. Their spatial pattern will again reflect relative importance of the dimerizations: in the WS the spins with $S=1/2$ will be present in every other site, while spin $S=1/2$ will be on the dimers if the dimerization is strong. In the presence of both V and dimerization the intermediate situations of the partial CO are realized, as has been demonstrated by the results of HF calculations as shown in Fig. 31 [97]. The antiferromagnetic pattern observed in some TMTTF compounds [98] is actually of the type shown in this figure, and the partial CO has been experimentally observed in different but similar systems (DI–DCNQI)$_2$Ag [99]. The spin degree of freedom in such a localized state can be represented by the quasi-one-dimensional antiferromagnetic Heisenberg model with $S=1/2$ with both the coupling to the lattice, λ, and interchain superexchange interaction $J_\perp$. If the former is dominant the SP state is realized, but as the latter gets important, e.g. by the external pressure, it is believed that there will be a first order phase transition from the SP state to the AF state [100]. On further increase of the pressure the degree of the localization will be reduced as deduced from the suppression of T_ρ in Fig. 30, and the ground state is transformed to SDW state. The difference between AF state and SDW state will be characterized as follows: in the AF state the localization of the charge sets in independently of the magnetic ordering, while SDW state emerges out of the metallic state but can be insulating once SDW state sets in, because of the opening of the gap everywhere over the Fermi surface as in the present case,

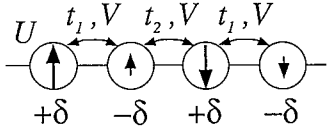

Figure 31 A schematic representation of the HF result for (TMTCF)2X. Transfer integrals along the TMTCF chains, $t1$ and $t2$, and the on-site and intersite Coulomb energies, U and V, are indicated, while δ denotes the CO and the length of the arrows schematically represent the amount of magnetic moment on the corresponding site.

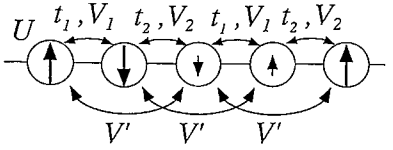

Figure 32 A schematic representation of the HF calculation corresponding to the $2k_F$ CDW and $2k_F$ SDW coexisting state in $(TMTSF)_2PF_6$.

where there is only one band with high degree of nesting. (Note that the system may stay in metallic state if there exist other Fermi surfaces left as in the cases in some of the heavy electron systems [101].) Another interesting feature found only recently is the coexistence of $2k_F$ CDW and SDW in $(TMTSF)_2PF_6$ [102]. A theoretical model has been proposed [103] for this unexpected phenomenon, which stresses the importance of long range Coulomb interaction not only between the nearest neighbors, V, but also those between the next nearest neighbors, V'. The expected charge and spin density modulations are as shown in Fig. 32. As seen in Fig. 30, the SC sets in concomitantly with the collapse of the SDW state. There exist indications that the symmetry of order parameter of this SC state is not BCS like but with line of nodes [104]. If this is the case, the Coulomb interactions leading to SDW should be playing essential roles to the stability of this SC state.

3.4. $(ET)_2X$

This family has many polytypes with a variety of ground state, some of which will be discussed in the following. The crystal structures of these are basically the same, i.e. composed of two-dimensional ET layers, but spatial arrangements of ET molecules in a unit cell are different, which result in drastically different ground states as described below.

3.4.1. α-$(ET)_2I_3$

Experimentally the temperature dependence of resistivity of this system have interesting features, i.e. at ambient pressure the resistivity sharply rises at around 50 K as T is lowered but with apparently finite limiting value towards $T=0$ (i.e. finite conductivity), while at $p=12$ kbar the temperature dependence of the resistivity is metallic towards $T=0$ [105]. In the almost insulating state at low temperature at ambient pressure, the spin susceptibility is suppressed isotropically indicating non-magnetic ground state [106]. This polytype has 4 ETs in a unit cell, whose spatial arrangement is shown in Fig. 33 schematically where each circle represents ET molecule and the values of the overlap integrals between the same HOMO orbitals of neighboring molecules are indicated. The resulting band structures and Fermi surfaces are shown in Fig. 34. As seen, all of

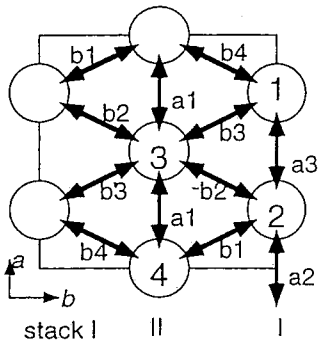

a1	3.0×10^{-3}
a2	4.9
a3	-1.8
b1	-12.3
b2	-14.2
b3	-6.2
b4	-2.3

Figure 33 A schematic view of the structure of the ET plane in α-$(ET)_2I_3$.

the four bands are weakly separated and the Fermi level corresponding to the $ET^{+1/2}$ is located roughly between top-most and the next top bands. In reality there can be a finite overlap between these two bands depending on the choice of the transfer integrals. The HF calculations with only U predict the phase diagram as shown in Fig. 35 [107], where the abscissa is the value of the transfer integral t_{b4}, which turns out to be the key factor to determine the degree of band overlap. It is inferred that this system is located in a very subtle region of the parameters. Beside the possibility of antiferromagnetic metals (AFM), the antiferromagnetic insulating (AFI) state has one-dimensional arrays of spin (with close to $S=1/2$) caused by CT between columns. Hence the comparison between theoretical predictions and experimental results may lead to the possibility of the SP ground state at ambient pressure accompanying the formation of the localized spins along the c-axis caused by the CO.

3.4.2. κ-$(ET)_2X$

This system, which also has 4 ETs in a unit cell, exhibits a phase diagram as shown in Fig. 36 with an interesting feature of having boundaries between AFI and SC [108]. There exist indications that the symmetry of this SC state is

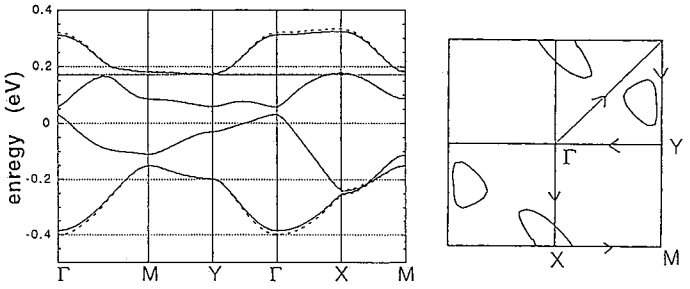

Figure 34 Band structure and Fermi surface of α-$(ET)_2I_3$.

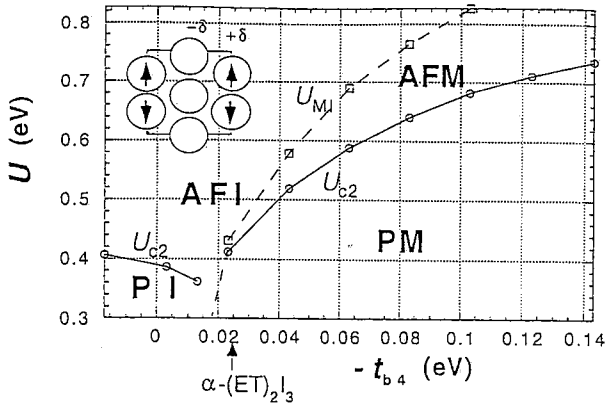

Figure 35 The HF phase diagram of α-$(ET)_2I_3$-type structure on the plane of t_{b4} and U.

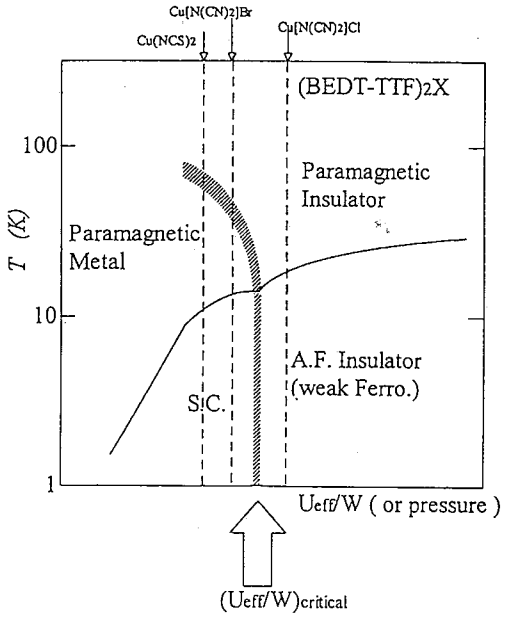

Figure 36 Phase diagram of κ-$(ET)_2X$ proposed by Kanoda [108].

different from that of BCS [109]. The locations of ET molecules in a unit cell are as in Fig. 37 where the overlap integrals between molecules are also indicated. As seen the overlap integral b_1 is larger than any others implying the formations of the dimerizations between two molecules connected by this b_1. Actually, as seen in Fig. 38 the band structures in the paramagnetic state is such that there exists a clear band-gap between second and third bands indicating that higher two and lower two bands are due to the anti-bonding and bonding orbitals within the

dimers, respectively. The crucial parameter, then, characterizing the system is the degree of dimerization represented by b_1. The HF phase diagram on the plane of this b_1 and U is shown in Fig. 39 [110]. The AFI in this case is same as the antiferromagnetism of spin $S = 1/2$ on each dimer. Once the effective value of U, i.e. U/W, is reduced by pressure, Fig. 39 predicts the transition from AFI to paramagnetic metals (PM), which will be SC as in the case of $(TMTCF)_2X$, Fig. 30.

3.4.3. α-$(ET)_2MHg(SCN)_4$

The spatial arrangement of ETs in this system is shown in Fig. 40 together with the overlap integrals leading to the extended Huckel band structures shown in Fig. 41. As seen this system is intermediate between α-$(ET)_2I_3$ and κ-$(ET)_2X$; if the degree of dimerization in κ-$(ET)_2X$ and the degree of the band-overlap in α-$(ET)_2I_3$ are varied, this system is realized [111]. This is schematically shown in Fig. 42(a). This affords a unified view on these three different polytypes. At the same time the phase diagram expected from this HF calculations is shown in Fig. 42(b) [111].

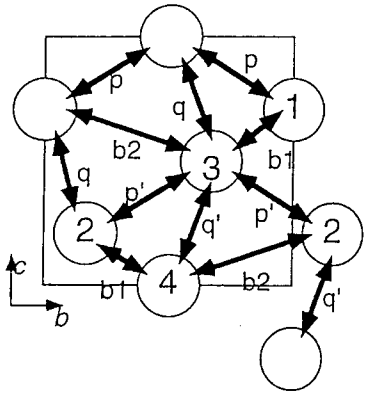

Figure 37 A schematic view of the structure of the ET plane in κ-$(ET)_2X$.

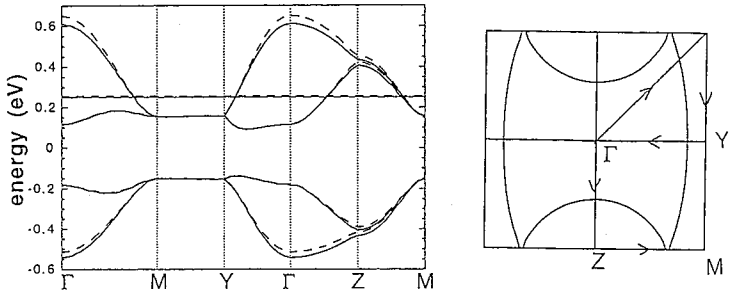

Figure 38 Band structure and Fermi surface of κ-$(ET)_2X$.

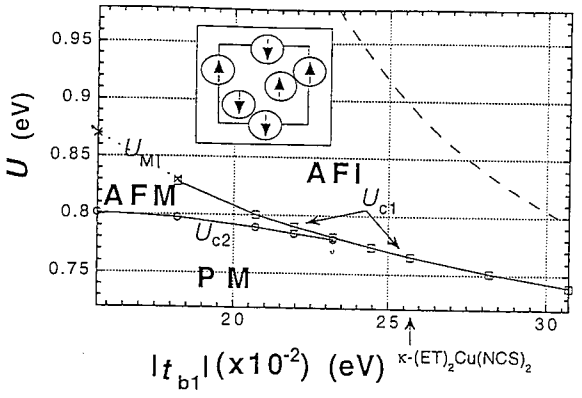

Figure 39 The HF phase diagram of κ-$(ET)_2X$-type structure on the plane of $|t_{b1}|$ and U.

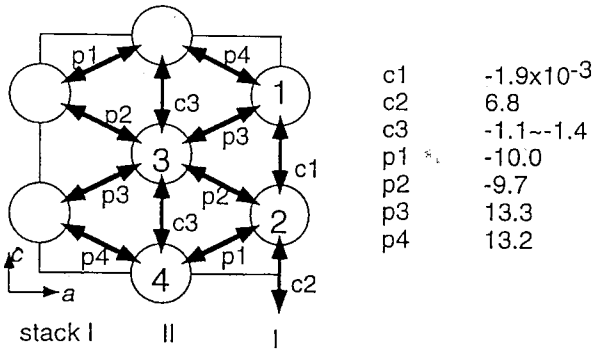

Figure 40 A schematic view of the structure of the ET plane in α-$(ET)_2MHg(SCN)_4$.

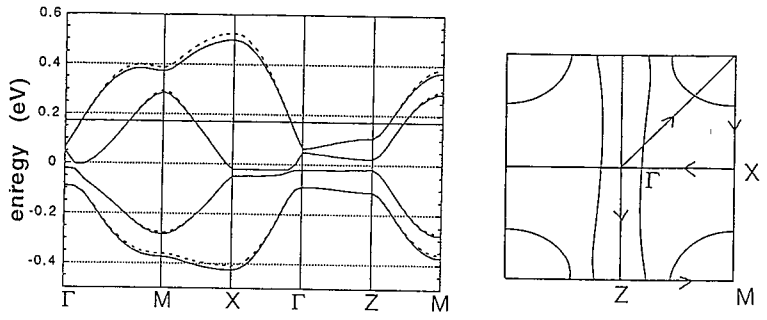

Figure 41 Band structure and Fermi surface of α-$(ET)_2MHg(SCN)_4$.

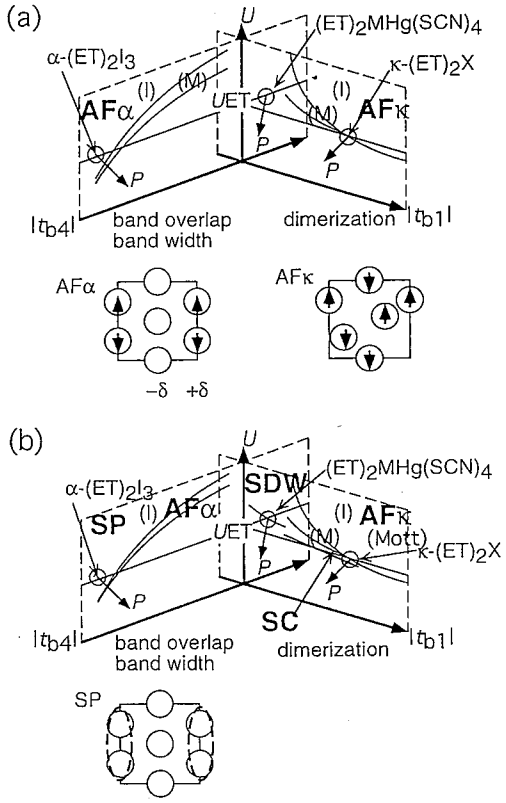

Figure 42 The HF (a) and expected (b) phase diagram for κ-$(ET)_2X$, α-$(ET)_2I_3$ and α-$(ET)_2MHg(SCN)_4$-types. AF_κ and Af_α are the AF ordered phases for the κ and α-type stuctures, respectively. (I) and (M) imply insulating and metallic phases, respectively. Arrows with P designate the effect of the applied pressure.

3.4.4. λ-(BETS)$_2$X

This family with $X = GaX_zY_{4-z}$ has 4 BETS molecules in a unit cell as in the case of $(ET)_2X$. Experiments have disclosed that the phase diagram of this system shares common features with κ-$(ET)_2X$ but with remarkable difference, i.e. the insulating state next to the SC state is non-magnetic here in contrast to the AFI state in κ-$(ET)_2X$ [112]. This can be understood theoretically as follows. The spatial arrangement of BETS molecules is schematically shown in Fig. 43 together with the transfer integrals. As seen the transfer integral, t_A, is larger than others leading to the possible formation of the dimers between BETS1 and BETS2. Actually the HF calculations leads to the antiferromagnetic ground state, where magnetization on BETS1 and BETS2 are parallel but antiparallel to those on BETS3 and BETS4 [113]. The magnitude of spin moments is dependent on U and the sum of those on BETS1 and BETS2 is close to $S = 1/2$ for the value of

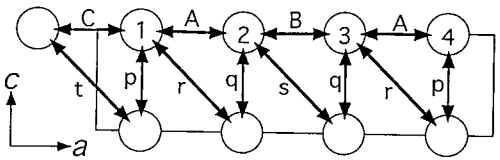

t_A 0.274 eV t_p -0.021 eV
t_B 0.111 eV t_q -0.040 eV
t_C 0.080 eV t_r 0.034 eV
t_s 0.049 eV
t_t 0.0065 eV

Figure 43 A schematic view of the structure of the BETS plane in λ-$(BETS)_2GaX_zY_{4-z}$.

U expected for these systems. These spins are aligned antiferromagnetically in the HF approximation as in Fig. 44. However this HF approximation ignores the quantum fluctuations of these spins, which in some cases play crucial roles. Such effects of quantum fluctuations will be properly incorporated by mapping this situation to the Heisenberg spin Hamiltonian where the localized spins with $S = 1/2$ are on the dimers and these spins are interacting by the superexchange interactions between them. In the present case these superexchange interactions are estimated by use of the original transfer integrals between molecules. The results are shown in Fig. 45. There exist the dimerizations in the resultant superexchange interactions, i.e. $J_B \neq J_C$, together with non-negligible $J_\perp$. The

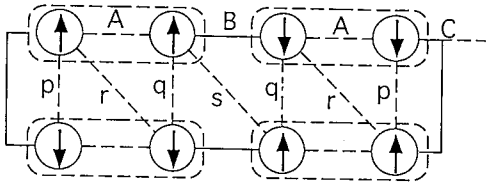

Figure 44 A schematic representation of the HF results for λ-$(BETS)_2GaX_zY_{4\mp z}$.

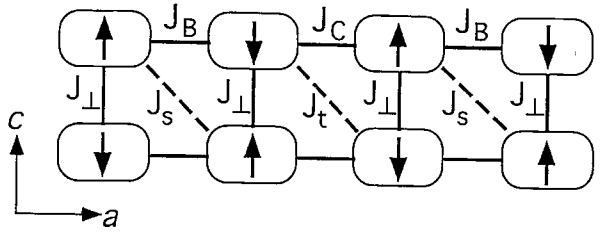

Figure 45 Effective two-dimensional Heisenberg model for localized spins in the dimer model for λ-$(BETS)_2GaX_zY_{4-z}$.

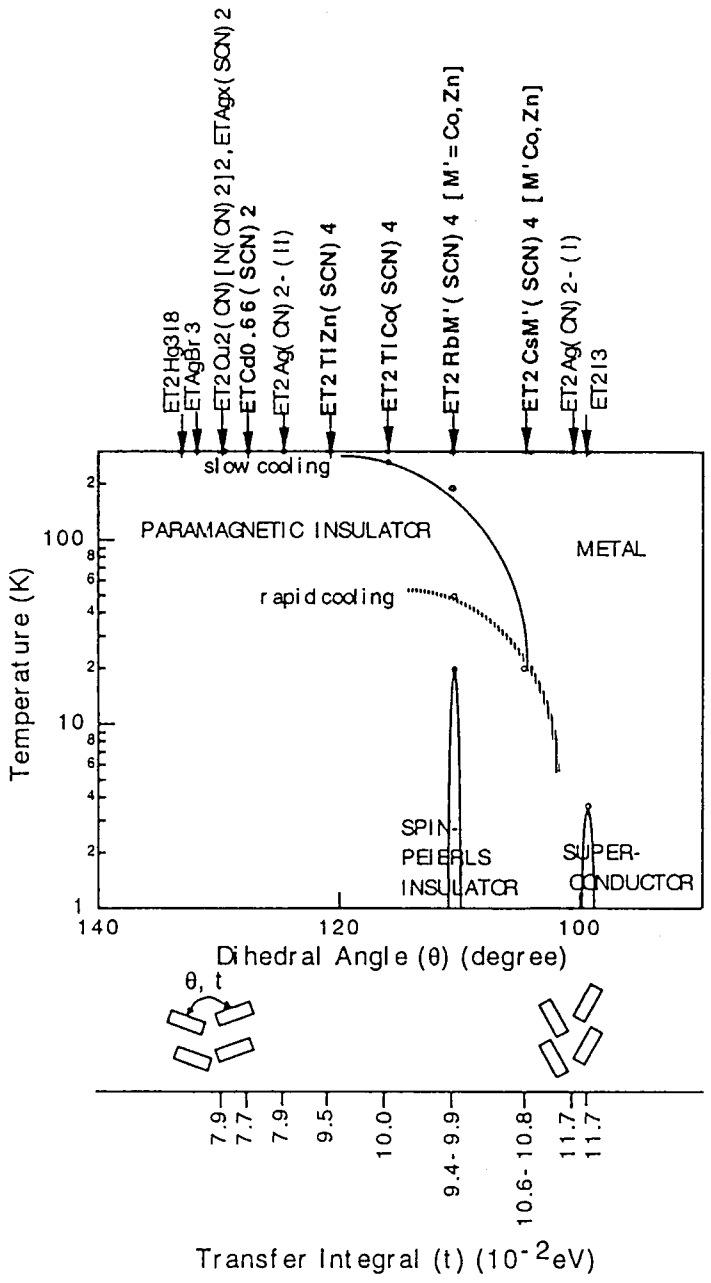

Figure 46 Phase diagram for θ-type ET salts proposed by Mori et al. [107], as a function of a transfer in the transverse direction (t) and the dihedral angle of donor columns.

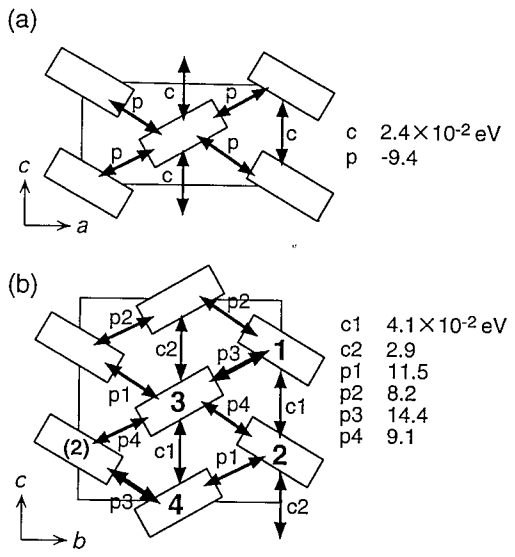

Figure 47 A schematic view of the structure of the ET plane in θ-$(ET)_2RbZn(SCN)_4$ in the high-temperature (a) and the slowly cooled low-temperature (b) phases.

phase diagram of such a spin system in two-dimension has been studied [114], where the ground states are either AF state or singlet state with a finite energy gap for the spin excitations, i.e. the SG state. From this, it will be argued that λ-BETS system is located very close to the boundary between the AF state and SG state, the latter of which is the candidate here [113]. If this is the case, the transformation to the AF state will be possible by small perturbations. Especially

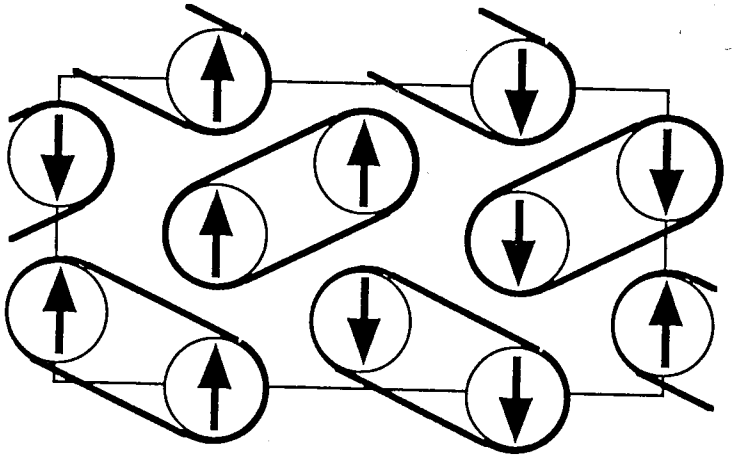

Figure 48 A schematic representation of the HF results for θ-$(ET)_2RbZn(SCN)_4$. The ellipses denote the dimers.

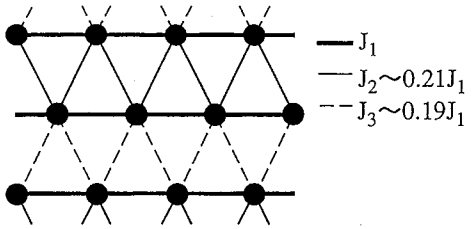

Figure 49 Effective two-dimensional Heisenberg model for localized spins in the dimer model for θ-$(ET)_2RbZn(SCN)_4$.

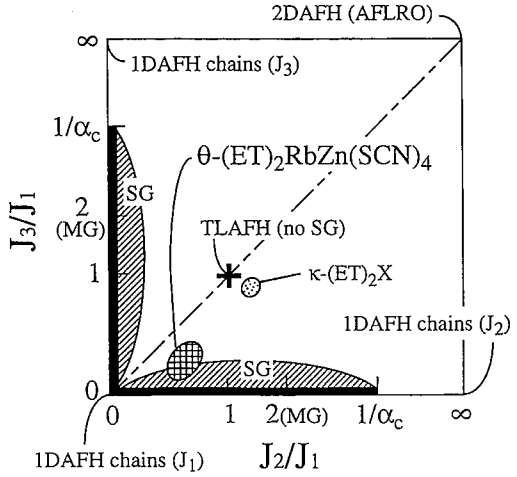

Figure 50 The schematic phase diagram of the Heisenberg spin model described in Fig. 49. It is symmetric with respect to the dot dashed line. SG, nDAFH, TLAFH, AFLRO and MG represent spin gap, *n*-dimensional antiferromagnetic Heisenberg model, triangular lattice antiferromagnetic Heisenberg model, antiferromagnetic long-range order and the Majumdar–Ghosh point, respectively. The regions where a spin gap is known to exist and where a spin gap is expected to exist are shown by the thick lines and the shaded area, respectively.

the effects of small amount of chemical impurities are of interest, as has been demonstrated in the case of disordered spin-Peierls systems [115]. In another member of this family with $X = FeX_zY_{4-z}$ the extra factors due to the localized spins of Fe^{3+} introduce another interesting interplay between SC and magnetism, whose microscopic mechanism has not yet been fully explored [116].

3.4.5. θ-$(ET)_2X$

This family, which has 2 ETs in a unit cell, has a phase diagram as shown in Fig. 46 [117]. Above all, in the case of θ-$(ET)_2RbZn(SCN)_4$, which is sensitive to the thermal variations, the dimerization resulting in the doubling of the unit cell sets

in as the temperature is lowered slowly as shown in Fig. 47 and the ground state is insulating and non-magnetic [117]. The results of the HF calculations for this system are shown in Fig. 48 [118]. As in λ-BETS there exists spin $S = 1/2$ on each dimer, which will be described by the Heisenberg spin model with the effective superexchange interactions as shown in Fig. 49. As seen the existence of the non-magnetic ground state in this case is obviously not due to the dimerizations of superexchange interaction. Instead, it will be due to the frustration. Actually the phase diagram of such frustrated spin models are expected to have rich structures as shown in Fig. 50 [119]. This system is expected be in the shaded region in the figure.

Recent results of similar calculations for $(ET)_2X$ including both intersite and onsite Coulomb interaction [121] predict that the ground state of α-$(ET)_2I_3$ is a CO state with the "stripe" pattern along the *b*-axis, rather than that along the *c*-axis as shown in an inset of Fig. 35 deduced when only onsite *U* is taken into account on one hand, and that the ground state of θ-type is also CO state with the "stripe" pattern along t_{p4}, rather than the Mott insulating state as shown in Fig. 47(b) suggested when only U is included. These indicate that the CO will be rather general in the presence of Coulomb interaction of finite range, which deserves further detailed studies.

3.5. Summary and Discussions

The results of recent theoretical studies searching for systematic understanding of the variety of ground states realized in $(TMTCF)_2X$ and $(ET)_2X$ salts are introduced. Based on the spin dependent Hartree–Fock approximation for the Coulomb interaction together with the extended Huckel type of the band structure calculations, the key parameters characterizing each family (polytype) are extracted resulting in the coherent understanding of the apparently unrelated types of the ground states. The calculations so far, however, have been limited to cases where only one molecular orbital, either LUMO or HOMO, is relevant. There exist another interesting cases where the overlap between LUMO and HOMO orbitals appears to be important as in dmit compounds [120] or the mixing between π-orbital and d-orbital plays crucial roles as in $(DCNQI)_2Cu$. In these cases one can expect richer possibilities, which are just being explored.

References

[1] As a review see for example, J. Wosnitza, Fermi Surfaces of Low-Dimensional Organic Metals and Superconductors, Springer Tracts in Modern Physics Vol. 134 Springer, Berlin, 1996.
[2] As a review see for example, S. Kagoshima, J. de Phys. I, 6 (1996) 1787.
[3] S. Kagoshima, H. Nagasawa, T. Sambongi, One-Dimensional Conductors, Springer series in solid-state science Vol. 72 Springer-Verlag, Berlin, 1988.
[4] As a review see for example, T. Ishiguro, K. Yamaji, and G. Saito, Organic Superconductors, Springer, 1998.

[5] As a review see for example, J.M. Williams, J.R. Ferraro, R.J. Thorn, K.D. Carlson, U. Geiser, H.H. Wang, A.M. Kini, and M-H. Whangbo, Organic Superconductors (Including Fullerenes), Prentice Hall, Englewood Cliffs, New Jersey, 1992.
[6] S. Uji, T. Terashima, H. Aoki, J.S. Brooks, R. Kato, H. Sawa, S. Aonuma, M. Tamura, and M. Kinoshita, Phys. Rev. B, 50 (1994) 15597.
[7] R. Kato, H. Kobayashi, H. Kim, A. Kobayashi, Y. Sasaki, T. Mori, and H. Inokuchi, Chem. Lett., (1988) 865.
[8] A. Kobayashi, T. Naito, and H. Kobayashi, Phys. Rev. B, 51 (1995) 3198.
[9] T. Inabe and K. Morimoto, Mol. Cryst. Liq. Cryst., 285 (1996) 107.
[10] R.P. Shibaeva, V.F. Kaminskii, V.K. Bel'skii, Krystallografiya, 29 (1984) 1089; Sov. Phys. Crystallogr. (Engl. Transl.) 29 (1984) 638. H.H. Wang, M.A. Beno, U. Geiser, M.A. Firestone, K.S. Webb, L. Nuñez, G.W. Crabtree, K.D. Carlson, J.M. Williams, L.J. Azevedo, J.F. Kwak, and J.E. Schirber, Inorg. Chem., 24 (1985) 2465. M-H. Whangbo, J.M. Williams, A.J. Schultz, T.J. Emge, and M.A. Beno, J. Am. Chem. Soc., 109 (1987) 90.
[11] T. Mori, A. Kobayashi, Y. Sasaki, H. Kobayashi, G. Saito, and H. Inokuchi, Bull. Chem. Soc. Jpn., 57 (1984) 627.
[12] H. Kobayashi, R. Kato, A. Kobayashi, Y. Nishio, K. Kajita, and W. Sasaki, Chem. Lett., (1986) 833.
[13] H. Mori, S. Tanaka, and T. Mori, Phys. Rev. B, 57 (1998) 12023.
[14] K. Bender, I. Hennig, D. Schweitzer, K. Dietz, H. Endres, H.J. Keller, Mol. Cryst. Liq. Cryst., 108 (1984) 359.
[15] H. Mori, S. Tanaka, M. Oshima, G. Saito, T. Mori, Y. Maruyama, and H. Inokuchi, Bull. Chem. Soc. Jpn., 63 (1990) 2183.
[16] H. Kino and H. Fukuyama, J. Phys. Soc. Jpn., 65 (1996) 2158.
[17] A. Kobayashi, R. Kato, H. Kobayashi, S. Moriyama, Y. Nishio, K. Kajita, and W. Sasaki, Chem. Lett., (1987) 459. R.N. Lyubovskaya, E.I. Zhilyaeva, S.I. Pesotskii, R.B. Lyubovskii, L.O. Atovmyan, O.A. D'yachenko, and T.G. Takhirov, JETP Lett., 46 (1987) 188. M. Kurmoo, D.R. Talham, K.L. Pritchard, P. Day, A.M. Stringer, and J.A.K. Howard, Synth. Met., 27 (1988) A177. A.M. Kini, U. Geiser, H.H. Wang, K.D. Carlson, J.M. Williams, W.K. Kwok, K.G. Vandervoort, J.E. Thompson, D.L. Stupka, D. Jung, and M-H. Whangbo, Inorg. Chem., 29 (1990) 2555.
[18] K. Kanoda, Hyperfine Interact., 104 (1997) 235.
[19] As a review see for example, G.C. Papavassiliou, A. Terzis, and P. Delhaes, Chapter 3, in: Handbook of Organic Conductive Molecules and Polymers, Vol. 1, Ed. by H.S. Nalwa, John Wiley & Sons Ltd, (1997).
[20] R. Kato, H. Kobayashi, A. Kobayashi, and Y. Sasaki, Chem. Lett., (1984) 1693.
[21] R. Kato, H. Kobayashi, and A. Kobayashi, Synth. Met., 41/43 (1991) 2093.
[22] H. Kobayashi, H. Tomita, T. Naito, A. Kobayashi, F. Sakai, T. Watanabe, and P. Cassoux, J. Am. Chem.Soc., 118 (1996) 368.
[23] H. Kobayashi, H. Akutsu, E. Arai, H. Tanaka, and A. Kobayashi, Phys. Rev. B, 56 (1997) R8526..
[24] Y. Misaki, N. Higuchi, T. Ohta, H. Fujiwara, T. Yamabe, T. Mori, H. Mori, and S. Tanaka, Mol. Cryst. Liq. Cryst., 284 (1996) 27.
[25] T. Kawamoto, Y. Misaki, K. Kawakami, H. Fujiwara, T. Yamabe, H. Mori, and S. Tanaka, Mol. Cryst. Liq. Cryst., 284 271 (1996).
[26] Y. Misaki, N. Higuchi, H. Fujiwara, T. Yamabe, T. Mori, H. Mori, and S. Tanaka, Angew. Chem. Int. Ed. Engl., 34 (1995) 1222.
[27] T. Mori, T. Kawamoto, J. Yamaura, T. Enoki, Y. Misaki, T. Yamabe, H. Mori, and S. Tanaka, Phys. Rev. Lett., 79 1702 (1997).
[28] G.C. Papavassiliou, D.J. Lagouvardos, A. Terzis, C.P. Raptopoulou, B Hilti, W. Hofherr, J.S. Zambounis, G. Rihs, J. Pfeiffer, P. Delhae, K. Murata, N.A. Fortune, and N. Shirakawa, Synth. Met., 70 (1995) 787. J.S. Zambounis, J. Pfeiffer, G.C. Papavassiliou, D.J. Lagouvardos, P. Delhae, L. Ducasse, N.A. Fortune, and K. Murata, Solid State Commun., 95 (1995) 211.
[29] E.B. Yagubskii, A.I. Kotov, E.E. Laukhina, A.A. Ignatiev, L.I. Buravov, and A.G. Khomenko, Synth., Met., 42 (1991) 2515. E.B. Yagubskii, L.A. Kushch, V.V. Gritsenko, O.A. Dyachenko, L.I. Buravov, and A.G. Khomenko, Synth. Met., 70 (1995) 1039.
[30] A. Aumüller, P. Erk, G. Klebe, S. Hünig, J.U. von Schütz, and H.-P. Werner, Angew. Chem. Int. Ed. Engl., 25 (1986) 740. R. Kato, H. Kobayashi, A. Kobayashi, T. Mori, and H. Inokuchi, Chem. Lett., (1987) 1579. R. Kato, H. Kobayashi, and A. Kobayashi, J. Am. Chem. Soc., 111 (1989) 5224. S. Hünig and P. Erk, Adv. Mater., 3 (1991) 225.
[31] I.H. Inoue, A. Kakizaki, H. Namatame, A. Fujimori, A. Kobayashi, R. Kato, and H. Kobayashi, Phys. Rev. B, 45 (1992) 5828.
[32] T. Miyazaki, K. Terakura, Y. Morikawa, and T. Yamasaki, Phys. Rev. Lett., 74 (1995) 5104.
[33] R. Kato, K. Yamamoto, Y. Okano, H. Tajima, and H. Sawa, Chem. Commun., (1997) 947.
[34] A. Kobayashi, R. Kato, H. Kobayashi, T. Mori, and H. Inokuchi, Solid State Commun., 64 (1987) 45. Y. Nogami, S. Hayashi, K. Oshima, K. Hiraki and K. Kanoda, Rev. High Pressure Sci. Technol. 7 (1998) 404. Y. Nogami, Y. Yamamoto, S. Hayashi, K. Oshima, K. Hiraki and K. Kanoda, Synth. Met., 103 (1999) 2252.
[35] S. Tomic, D. Jérome, A. Aumüller, P. Erk, S. Hünig, and J.U. von Schütz, Synth. Met., 27 (1988) B281.
[36] S. Hünig, K. Sinzger, M. Jopp, D. Bauer, W. Bietsch, J.U. von Schütz, and H.C. Wolf, Angew. Chem. Int. Ed. Engl., 31 (1992) 859. K. Sinzger, S. Hünig, M. Jopp, D. Bauer, W. Bietsch, J.U. von Schütz, and H.C. Wolf, R.K. Kremer, T. Metzenthin, R. Bau, S.I. Khan, A. Lindbaum, C.L. Lengauer, and E. Tillmanns, J. Am. Chem. Soc., 115 (1993) 7696. S. Aonuma, H. Sawa, and R. Kato, J. Chem. Soc. Perkin Trans. 2 (1995) 1541.
[37] R. Kato, S. Aonuma, and H. Sawa, Mol. Cryst. Liq. Cryst., 284 (1996) 183.
[38] O. Akaki, A. Chainani, T. Takahashi, Y. Kashimura, and R. Kato, Phys. Rev. B, 57 (1998) 11846.
[39] H. Fukuyama, Synth. Met., 71 (1995) 1861. H. Fukuyama, J. Phys. Soc. Jpn., 61 (1992) 3452. T. Ogawa and Y. Suzumura, J. Phys. Soc. Jpn., 63 (1994) 2066.
[40] Y. Kashimura, H. Sawa, S. Aonuma, R. Kato, H. Takahashi, and N. Môri, Solid State Commun., 93 (1995) 675. R. Kato, Y. Kashimura, S. Aonuma, H. Sawa, H. Takahashi, and N. Môri, Mol. Cryst. Liq. Cryst., 285 (1996) 143.
[41] T. Miyazaki and K. Terakura, Phys. Rev. B, 56 (1997) R477.
[42] R. Kato, Y-L. Liu, Y. Hosokoshi, S. Aonuma, and H. Sawa, Mol. Cryst. Liq. Cryst., 296 (1997) 217.
[43] A. Kobayashi, A. Sato, T. Naito, and H. Kobayashi, Mol. Cryst. Liq. Cryst., 284 (1996) 85.
[44] P. Cassoux, L. Valade, H. Kobayashi, A. Kobayashi, R.Ä. Clark, and A.E. Underhill, Coord. Chem. Rev., 110 (1991) 115. A. Kobayashi and H. Kobayashi, Chapter 5, in: Handbook of Organic Conductive Molecules and Polymers, Vol. 1 Ed. by H.S. Nalwa, John Wiley & Sons Ltd, 1997.
[45] E. Canadell, S. Ravy, J.P. Pouget, and L. Brossard, Solid State Commun., 75 (1990) 633. E. Canadell, I.E. -I. Rachidi, S. Ravy, J.P. Pouget, L. Brossard, and J.P. Legros, J. Phys. France, 50 (1989) 2967. H. Tajima, T. Naito, M. Tamura, A. Kobayashi, H. Kuroda, R. Kato, H. Kobayashi, R.A. Clark, and A.E. Underhill, Solid State Commun., 79 (1991) 337.
[46] M.Y. Ogawa, B.M. Hoffman, S. Lee, M. Yudkowsky, and W.P. Halperin, Phys. Rev. Lett., 57 (1986) 1177.
[47] T. Enoki, J-I. Yamaura, and A. Miyazaki, Bull. Chem. Soc. Jpn., 70 (1997) 2005.
[48] M. Kurmoo, A.W. Graham, P. Day, S.J. Coles, M.B. Hursthouse, J.L. Caulfield, J. Singleton, F.L. Pratt, W. Hayes, L. Ducasse, and P. Guionneau, J. Am. Chem. Soc., 117 (1995) 12209.
[49] F. Gose, V.N. Laukhin, L. Brossard, A. Audouard, J.P. Ulmet, S. Askenazy, T. Naito, H. Kobayashi, A. Kobayashi, M. Tokumoto, and P. Cassoux, Europhys, Lett., 28 (1994) 427.
[50] See for example, J. Bernasconi, P. Bruesch and H.R. Zeller, J. Phys. Chem. Solid, 35 (1974) 145. H.R. Zeller and A. Beck, J. Phys. Chem. Solid 35 (1974) 77.
[51] See for example, F. Wudl, G.M. Smith and E.J. Hufnagel, J.C.S. Chem. Commun. (1970) 1453. J.P. Ferraris, D.O. Cowan, V. Walatka, Jr. And J.H. Perlstein, J. Am. Chem. Soc., 95 (1973) 948. L.B. Coleman, M.J. Cohen, D.J. Sandman, F.G. Yamagishi, A.F. Garito and A.J. Heeger, Solid State Commun., 12 (1973) 1125.
[52] As review books see for example, J.P. Pouget and R. Comès, Charge Density Waves, in, Solids, Ed. L.P. Gor'kov and G. Gruner, in, Modern Problems in: Condensed Matter Sciences, Ed. V.M. Agranovich and A.A. Maradudin (North Holland; Amsterdam, Oxford, New York, Tokyo, 1989). S. Kagoshima, H. Nagasawa and T. Sambongi, One-Dimensional Conductors (Springer-Verlag, Berlin, Heidelberg, 1988). G. Gruner, Density Waves in Solids (Addison-Wesley, Massachusetts, 1994). J-P. Farges, Organic Conductors (Marcel Dekker, New York, Basel, Hong Kong, 1994).

[53] M.J. Cohen, L.B. Coleman, A.F. Garito and A.J. Heeger, Phys. Rev. B, 10 (1974) 1298. T. Ishiguro, S. Kagoshima and H. Anzai, J. Phys. Soc. Jpn., 41 (1976) 351. S. Etemad, Phys. Rev. B, 13 (1976) 2254. M.J. Cohen, and A.J. Heeger, Phys. Rev. B, 16 (1977) 688.
[54] A.A. Bright, A.F. Garito and A.J. Heeger, Solid State Commun., 13 (1973) 943. D.B. Tanner, C.S. Jacobsen, A.F. Garito and A.J. Heeger, Phys. Rev. B, 13 (1976) 3381. Y. Tomkiewicz, B.A. Scott, L.J. Tao and R.S. Title, Phys. Rev. Lett., 32 (1974) 1363. J.C. Scott, A.F. Garito and A.J. Heeger, Phys. Rev. B, 10 (1974) 3131. J.F. Kwak, P.M. Chaikin, A.A. Russel, A.F. Garito and A.J. Heeger, Solid State Commun., 16 (1975) 729. P.M. Chaikin, R.L. Greene, S. Etemad and E.M. Engler, Phys. Rev. B, 13 (1976) 1627.
[55] F. Denoyer, R. Comès, A.F. Garito and A.J. Heeger, Phys. Rev. Lett., 35 (1975) 445. S. Kagoshima, H. Anzai, K. Kajimura and T. Ishiguro, J. Phys. Soc. Jpn., 39 (1975) 1143.
[56] S. Kagoshima, T. Ishiguro and H. Anzai, J. Phys. Soc. Jpn., 41 (1976) 2061. J.P. Pouget, S.K. Khanna, F. Denoyer, R. Comès, A.F. Garito and A.J. Heeger, Phys. Rev. Lett., 37 (1976) 437. S.K. Khanna, J.P. Pouget, R. Comès, A.F. Garito and A.J. Heeger, Phys. Rev. B, 16 (1976) 1468.
[57] R. Comès, S.M. Shapiro, G. Shirane, A.F. Garito and A.J. Heeger, Phys. Rev. Lett., 35 (1975) 1518. W.D. Ellenson, R. Comès, S.M. Shapiro, G. Shirane, A.F. Garito and A.J. Heeger, Solid State Commun., 20 (1976) 53. R. Comès, G. Shirane, S.M. Shapiro, A.F. Garito and A.J. Heeger, Phys. Rev. B, 14 (1976) 2376. W.D. Ellenson, S.M. Shapiro, G. Shirane and A.F. Garito, Phys. Rev. B, 16 (1977) 3244.
[58] R.E. Peierls, Quantum Theory of Solids (Clarendon Press, Oxford, 1955) Chap. 5.
[59] W. Kohn, Phys. Rev. Lett., 2 (1959) 393. E.J. Woll, Jr. And W. Kohn, Phys. Rev., 126 (1962) 1693. M. Afanas'ev and Yu Kagan, Soviet Phys. JETP, 16 (1963) 1030.
[60] G. Shirane, S.M. Shapiro, R. Comès, A.F. Garito and A.J. Heeger, Phys. Rev. B, 14 (1976) 2325. J.P. Pouget, S.M. Shapiro, G. Shirane, A.F. Garito and A.J. Heeger, Phys. Rev. B, 19 (1979) 1792.
[61] W.D. Grobman and B.D. Silverman, Solid State Commun., 19 (1976) 319.
[62] P. Bak and V.J. Emery, Phys. Rev. Lett., 36 (1976) 978. T.D. Schultz and S. Etemad, Phys. Rev. B, 13 (1976) 4928. T.D. Schultz, Solid State Commun., 22 (1977) 289.
[63] As review books see for example, G. Gruner, Density Waves in Solids (Addison-Wesley, Massachusetts, 1994). P. Monceau, Electronic Properties of Inorganic Quasi-One-Dimensional Compounds (D. Reidel Publ. Co., Dordrecht, Boston, 1985).
[64] J.C. Scott, H.J. Pedersen, K. Bechgaard, Phys. Rev. Lett., 45 (1980) 2125. H.J. Pedersen, J.C. Scott, K. Bechgaard, Solid State Commun., 35 (1980) 207. W.M. Walsch, F. Wudl, G.A. Thomas, D. Nalewajek, J.J. Hauser, P.A. Lee, T. Poeeeehler, Phys. Rev. Lett., 45 (1980) 829. A. Andieux, D. Jérome and K. Bechgaard, J. Phys. Lett. (Paris), 43 (1981) L87.
[65] J.P. Pouget and S. Ravy, J. Phys. I, 6 (1996) 1501. J.P. Pouget and S. Ravy, Synth. Met., 85 (1997) 1523.
[66] N. Kobayashi, M. Ogata and K. Yonemitsu, J. Phys. Soc. Jpn., 67 (1998) 1098.
[67] J. Kondo and K. Yamaji, J. Phys. Soc. Jpn., 43 (1977) 424.
[68] S. Kagoshima, J. Phys. Soc. Jpn., suppl. A (1980) 857.
[69] As a review see for example, J.W. Bray, L.V. Interrante, I.S. Jacobs and J.C. Bonner, Extended Linear Chain Compounds, Vol. III, Ed. J.S. Miller (Plenum Press, New York and London, 1983).
[70] S. Huizinga, J. Kommandeur, G.A. Sawatzky, K. Kopinga and W.J.M. de Jonge, Quasi One-Dimensional Conductors II, Ed. S. Barisic, A. Bjelis, J.R. Cooper and B. Lentic (Springer-Verlag, Berlin, Heidelberg, New York, 1979) pp.45.
[71] J.C. Bonner and M.E. Fisher, Phys. Rev., 135 (1964) A640.
[72] B. van Bodegom, B.C. Larson and H.A. Mook, Phys. Rev. B, 24 (1981) 1520.
[73] S. Inagaki and H. Fukuyama, J. Phys. Soc. Jpn., 52 (1983) 2504. Ibid, 3620. J. Kondo, Physica, 123B (1984) 169.
[74] D. Jérome, Science, 252 (1991) 1509 Organic Conductors, ed, J-P. Farge (Marcel Dekker, 1994) p.420.
[75] R. Moret, J.P. Pouget, R. Comès and K. Bechgaard, Phys. Rev., 49 (1982) 1008. J.P. Pouget, G. Shirane, K. Bechgaard, J.M. Fabre, Phys. Rev. B, 27 (1983) 5203.
[76] J.P. Pouget and S. Ravy, J. Phys. I, 6 (1996) 1501.

[77] S. Kagoshima, T. Yasunaga, T. Ishiguro, H. Anzai and G. Saito, Solid State Commun., 46 (1983) 867. J.P. Pouget, S. Kagoshima, T. Tamegai, Y. Nogami, K. Kubo, T. Nakajima and K. Bechgaard, J. Phys. Soc. Jpn. 59 (1990) 2036.
[78] S.S.P. Parkin, M. Ribault, D. Jérome, K. Bechgaard, J. Phys. (Paris), C14 (1981) L445.
[79] S. Tomic, D. Jérome, A. Aumuller, P. Erk, S. Hünig and J.U. von Schutz, J. Phys. C, 21 (1988) L203.
[80] A. Kobayashi, T. Mori, H. Inokuchi, R. Kato and H. Kobayashi, Synth. Met., 27 (1988) B275.
[81] R. Moret, Synth. Met., 27 (1988) B301.
[82] R. Kato, S. Aonuma and H. Sawa, Mol. Cryst. Liq. Cryst., 284 (1996) 183.
[83] H. Fukuyama, J. Phys. Soc. Jpn., 61 (1992) 3452.
[84] M. Nakano, M. Kato, and K. Yamada, Physica B, 186 (1993) 1077.
[85] T. Miyazaki, K. Terakura, Y. Morikawa and T. Yamasaki, Phys. Rev. Lett. 74 (1995) 5104.
[86] S. Uji, T. Terashima, H. Aoki, J.S. Brooks, R. Kato, H. Sawa, S. Aonuma, M. Tamura and M. Kinoshita, Phys. Rev. B 50 (1994) 15597.
[87] L.B. Coleman, M.J. Cohen, D.J. Sandman, F.F. Yamagishi, A.F. Gavito and A.J. Heeger, Solid State Commun. 12 (1973) 1125.
[88] e.g. Highly Conducting One-Dimensional Solids, Ed. J.T. Devreese, R.P. Evrard and V.E. van Doren (Plenum Press, New York and London, 1979).
[89] P.A. Lee, T.M. Rice and P.W. Anderson, Solid State Commun. 14 (1974) 703.
[90] H. Fukuyama, J. Phys. Soc. Jpn. 41 (1976) 513. H. Fukuyama and P.A. Lee, Phys. Rev. B 17 (1978) 535; P.A. Lee and T.M. Rice, Phys. Rev. B 19 (1979) 1370.
[91] A.W. Overhauser, Phys. Rev. Lett. 4 (1960) 462 Phys. Rev. 128 (1962) 1437; for a modern review, G. Gruner, Density Waves in Solid (Addison-Wesley, Massachusetts, 1994).
[92] For a review on anisotropic superconductivity, M. Sigrust and K. Ueda, Rev. Mod. Phys. 63 (1991) 239.
[93] M.C. Cross and D.S. Fisher, Phys. Rev. B 19 (1979) 402; T. Nakano and H. Fukuyama, J. Phys. Soc. Jpn. 49 (1980) 1679; for reviews, J.W. Bray, L.V. Interrante, I.S. Jacobs and J.C. Bonner, Extended Linear Chain Compounds, Ed. J.S. Miller (Plenum Press, New York and London, 1983) p. 353; H. Fukuyama and S. Inagaki, Magnetic Properties of Low-Dimensional Systems, ed. L.M. Falikov and J.L. Moran-Lopez (Springer Verlag, Berlin, Heidelberg and New York, 1986) p. 156.
[94] T. Mori, A. Kobayashi, Y. Sasaki, H. Kobayashi, G. Saito and H. Inokuchi, Bull. Chem. Soc. Jpn. 57 (1984) 627.
[95] e.g. D. Jérome, Physics and Chemistry of Low-Dimensional Inorganic Conductors, Ed. C. Schlenker et al., (Plenum Press, New York, 1996) 141.
[96] J.E. Hirsch and D.J. Scalapino, Phys. Rev. Lett. 50 (1983) 1168; Phys. Rev. B 27 (1983) 7169; ibid. 29 (1984) 5554. S. Mazumdar, S.N. Dixit and A.N. Bloch, Phys. Rev. B 30 (1984) 4842.
[97] H. Seo and H. Fukuyama, J. Phys. Soc. Jpn. 66 (1997) 1249.
[98] T. Nakamura, T. Nobutoki, Y. Kobayashi, T. Takahashi and G. Saito, Synth. Met. 70 (1995) 1293; T. Nakamura, R. Kinami, T. Takahashi and G. Saito, Synth. Met. 86 (1997) 2053.
[99] K. Hiraki and K. Kanoda, Phys. Rev. Lett. 80 (1998) 4737.
[100] S. Inagaki and H. Fukuyama, J. Phys. Soc. Jpn. 52 (1983) 3620.
[101] e.g. F.M. Grosche, S.R. Julien, N.D. Mathur and G.G. Lonzarich, Physica B 223–224 (1996) 50; S.R. Julien, C. Pfleiderer, F.M. Grosche, N.D. Mathur, G.J. McMullan, A.J. Diver, I.R. Walker and G.G. Lonzarich, J. Phys. Cond. Mat. 8 (1996) 9675.
[102] J.P. Pouget and S. Ravy, Synth. Met. 85 (1997) 1523; J. Phys. I 6 (1996) 1501.
[103] N. Kobayashi, M. Ogata and K. Yonemitsu, J. Phys. Soc. Jpn. 67 (1998) 1098.
[104] M. Takigawa, H. Yasuoka and G. Saito, J. Phys. Soc. Jpn. 56 (1987) 873; H. Hasegawa and H. Fukuyama, J. Phys. Soc. Jpn. 55 (1986) 3978; ibid. 56 (1987) 877.
[105] K. Kajita, T. Ojiro, H. Fujii, Y. Hishio, H. Kobayashi, A. Kobayashi and R. Kato, J. Phys. Soc. Jpn. 61 (1992) 23.
[106] B. Rothaemel, L. Forro, J.R. Cooper, JÅDS. Schiling, M. Weger, P. Bele, H. Brunner, D. Schweitzer and H.J. Keller, Phys. Rev. B 34 (1986) 704.
[107] H. Kino and H. Fukuyama, J. Phys. Soc. Jpn. 64 (1995) 1877.
[108] K. Kanoda, Hyperfine Interact. 104 (1997) 235.

[109] N. Mayaffre, P. Wzietek, D. Jérome, C. Lenoir and P. Batail, Phys. Rev. Lett. 75 (1995); Y. Nakazawa and K. Kanoda, Phys. Rev. B 55 (1997) 8670.
[110] H. Kino and H. Fukuyama, J. Phys. Soc. Jpn. 64 (1995) 2726.
[111] H. Kino and H. Fukuyama, J. Phys. Soc. Jpn. 64 (1995) 4523; ibid. 65 (1996) 2158.
[112] H. Kobayashi, H. Akutsu, E. Arai, H. Tanaka and A. Kobayashi, Phys. Rev. B 56 (1997) 8526.
[113] H. Seo and H. Fukuyama, J. Phys. Soc. Jpn. 66 (1997) 3352.
[114] N. Katoh and M. Imada, J. Phys. Soc. Jpn. 63 (1994) 4529; ibid. 64 (1995) 1437.
[115] H. Fukuyama, T. Tanimoto and M. Saito, J. Phys. Soc. Jpn. 65 (1996) 1183; H. Fukuyama, Hyperfine Interact. 104 (1997) 17.
[116] H. Akutsu, K. Kato, E. Ojima, H. Kobayashi, H. Tanaka, A. Kobayashi and P. Cassoux, Phys. Rev. B 58 (1998) 9294; L. Brosard, R. Clerac, C. Coulon, M. Tokumoto, T. Ziman, D.K. Petrov, V.N. Laukhin, M.J. Naughton, A. Audouard, F. Goze, A. Kobayashi, H. Kobayashi P. Cassoux, Eur. Phys.J. B 1 (1998) 439.
[117] H. Mori , S. Tanaka and T. Mori, Phys. Rev. B 57 (1998) 12023; H. Mori, S. Tanaka, T. Mori, A. Kobayashi and H. Kobayashi, Bull. Chem. Soc. Jpn. 71 (1998) 797
[118] H. Seo and H. Fukuyama, J. Phys. Soc. Jpn. 67 (1998) 1848.
[119] This general phase diagram was originally suggested to us by N. Katoh.
[120] M. Mori, K. Yonemistsu and H. Kino, to be published in J. Phys. Soc. Jpn.
[121] H. Seo and H. Fukuyama, Proceedings of LT22, Helsinki, August 1999 (to be published in Physica B); H. Seo, preprint, submitted to J. Phys. Soc. Jpn.

CHAPTER 5

Organic Lower-Dimensional Crystalline and Monolayer Conductors

Robert Melville Metzger

Department of Chemistry, University of Alabama, Tuscaloosa, AL 35487-0336, USA

In memorium: Pier Luigi Nordio (1936–1998) and Aaron N. Bloch (1942–1995): they helped us find the way.

1. Introduction and Early History

During the first six decades of the twentieth century interest in the solid-state properties of organic molecules and their ions was limited. Conventional organic solids have covalent chemical bonds within each molecule and only van der Waals or London interactions between molecules. It is relatively unusual to find partial or complete formal charges on constituent cations and anions, and therefore Coulomb interactions between organic molecules in crystals.

However, metallic conduction in organic systems had been dreamt of as early as 1911 [1]. Until the mid 1960s the serious researchers of the organic solid state were few: Hideo Akamatsu [2], Noel S. Bayliss [3], Melvin Calvin [4], Daniel D. Eley [5], Helmuth Kainer [6], Aleksandr I. Kitaigorodskii [7], Jan Kommandeur [8], Yoshio Matsunaga [9], Harden M. McConnell [10], Albert Szentgyörgyi [11], A.N. Terenin [12] and A.T. Vartanyan [12].

The landmark results, which propelled low-dimensional organic systems to the great level of present interest, have been a mix of experimental breakthroughs and theoretical ideas:

(1) superconductivity in potassium-intercalated graphite (1965) [13];